SUBMITTED TO APJ, FEBRUARY 13, 2006
Preprint typeset using LaTeX style emulateapj v. 6/22/04

THE RELATION BETWEEN QUASAR AND MERGING GALAXY LUMINOSITY FUNCTIONS AND THE MERGER-DRIVEN STAR FORMATION HISTORY OF THE UNIVERSE

PHILIP F. HOPKINS[1], RACHEL S. SOMERVILLE[2], LARS HERNQUIST[1], THOMAS J. COX[1], BRANT ROBERTSON[1], & YUEXING LI[1]

Submitted to ApJ, February 13, 2006

ABSTRACT

Using a model for the self-regulated growth of supermassive black holes in mergers involving gas-rich galaxies, we study the relationship between quasars and the population of merging galaxies and thereby predict the merger-driven star formation rate density of the Universe. In our picture, mergers drive gas inflows, fueling nuclear starbursts and "buried" quasars until feedback disperses the gas, allowing the quasar to be briefly visible as a bright optical source. As black hole accretion declines, the quasar dies and the stellar remnant relaxes passively with properties and correlations typical of red, elliptical galaxies. By simulating the evolution of such events, we demonstrate that the observed *statistics* of merger rates/fractions, luminosity functions, mass functions, star formation rate distributions, quasar luminosity functions, quasar host galaxy luminosity functions, and elliptical/red galaxy luminosity and mass functions are self-consistent. We use our simulations to de-convolve both the quasar and merging galaxy luminosity functions to determine the birthrate of black holes of a given final mass and merger rates as a function of the total stellar mass and the mass of new stars formed during a merger. From this, we predict the merging galaxy luminosity function in various observed wavebands (e.g. UV, optical, and near-IR), color-magnitude relations, mass functions, absolute and specific star formation rate distributions and star formation rate density, and quasar host galaxy luminosity function, as a function of redshift from $z = 0-6$. We invert this relationship to predict e.g. quasar luminosity functions from observed merger luminosity functions or star formation rate distributions. Our results show good agreement with observations, but idealized models of quasar lightcurves give inaccurate estimates and are ruled out by comparison of merging galaxy and quasar observations at $> 99.9\%$ confidence, provided that quasars are triggered in mergers. Using only observations of quasars, we estimate the contribution of mergers to the star formation rate density of the Universe to high redshifts, $z \sim 4$, and constrain the evolution in the characteristic initial gas fractions of quasar and spheroid-producing mergers.

Subject headings: quasars: general — galaxies: active — galaxies: evolution — cosmology: theory

1. INTRODUCTION

It is believed that our Universe evolved hierarchically, with small objects merging to form progressively larger systems. Observations of interacting galaxies support this view and led Toomre & Toomre (1972) and Toomre (1977) to propose the "merger hypothesis," according to which ellipticals originate when spiral galaxies collide (for reviews, see e.g. Barnes & Hernquist 1992; Barnes 1998; Schweizer 1998). It has also been established that supermassive black holes are ubiquitous in the centers of galaxies (e.g. Kormendy & Richstone 1995; Richstone et al. 1998; Kormendy & Gebhardt 2001) and that their masses correlate with either the masses (Magorrian et al. 1998) or the velocity dispersions (i.e. the $M_{\rm BH}$-σ relation: Ferrarese & Merritt 2000; Gebhardt et al. 2000) of their host spheroids. These relations argue that supermassive black holes and galaxies are linked in an evolutionary manner, as implied by simulations showing that self-regulated black hole growth in a galaxy merger has a significant impact on the structure of the remnant (Di Matteo et al. 2005).

Observations also indicate that galaxy mergers produce starbursts and fuel black hole growth, and that both play roles in structuring ellipticals. Infrared luminous galaxies appear to be powered at least in part by nuclear starbursts (e.g. Soifer et al. 1984a,b; Sanders et al. 1986, 1988a,b; for a review, see e.g. Soifer et al. 1987), and the most intense of these, ultraluminous infrared galaxies (ULIRGs), are always associated with mergers (e.g. Allen et al. 1985; Joseph & Wright 1985; Armus et al. 1987; Kleinmann et al. 1988; Melnick & Mirabel 1990; for reviews, see Sanders & Mirabel 1996 and Jogee 2005). Radio observations reveal large quantities of dense gas in the centers of ULIRGs (e.g. Scoville et al. 1986; Sargent et al. 1987, 1989), providing material to feed black hole growth and to boost the concentration and central phase space density to match those of ellipticals (see, e.g. Carlberg 1986; Gunn 1987; Lake 1989; Hernquist 1992, 1993a; Hernquist et al. 1993; Robertson et al. 2006a). Some ULIRGs have "warm" IR spectral energy distributions (SEDs), suggesting that they harbor buried quasars (e.g. Sanders et al. 1988c), as implied by X-ray observations of growing black holes in NGC6240 (Komossa et al. 2003) and other ULIRGs, which are heavily obscured at optical and infrared wavelengths (e.g. Gerssen et al. 2004; Max et al. 2005; Alexander et al. 2005a,b; Borys et al. 2005).

These lines of evidence, and the overlap between the bolometric luminosities of ULIRGs and quasars, suggest that quasars originate from an IR luminous phase of galaxy evolution caused by mergers (Sanders et al. 1988a). This proposal is supported by observations of nearby hosts of bright quasars which reveal features characteristic of mergers (e.g. Stockton 1978; Heckman et al. 1984; Stockton & MacKenty 1987; Stockton & Ridgway 1991; Hutchings & Neff 1992; Bahcall et al. 1994, 1995, 1997; Canalizo & Stockton 2001) and starbursts (e.g., Brotherton et al. 1999, 2002; Canalizo et al. 2000; Yip et al. 2004; Vanden Berk et al. 2006).

Observations of individual merging systems and merger

[1] Harvard-Smithsonian Center for Astrophysics, 60 Garden Street, Cambridge, MA 02138
[2] Max-Planck-Institut für Astronomie, Königstuhl 17, Heidelberg 69117, Germany

remnants (e.g., Lake & Dressler 1986; Doyon et al. 1994; Oliva et al. 1995; Shier & Fischer 1998; James et al. 1999) have shown that their kinematic and photometric properties, including velocity dispersions, concentrations, stellar masses, light profiles, and phase space densities, are consistent with their eventual evolution into typical $\sim L_*$ elliptical galaxies. Furthermore, the correlations obeyed by these mergers and remnants (e.g., Genzel et al. 2001; Rothberg & Joseph 2004, 2006) are similar to e.g. the observed fundamental plane and Kormendy relations for relaxed ellipticals, and consistent with evolution onto these relations as their stellar populations age.

While these studies suggest that nearby gas-rich mergers pass through starburst and quasar phases and evolve into ellipticals, the implications of these findings at higher redshifts are unclear and little is known about the *statistics* of galaxy mergers in this context. In particular, it is difficult to measure the detailed properties of distant quasar hosts (e.g., Schweizer 1982; Dunlop et al. 2003; Floyd et al. 2004), and it is not clear if there are enough mergers to account for the present abundance of spheroids or whether all gas-rich or elliptical-producing mergers undergo an infrared luminous starburst phase. The galaxy merger rate and its evolution has been estimated (e.g., Xu & Sulentic 1991; Burkley et al. 1994; Carlberg et al. 1994; Sulentic & Rabaca 1994; Keel & Wu 1995; Soares et al. 1995; Yee & Ellingson 1995; Patton et al. 1997; Zepf & Koo 1989; Toledo et al. 1999; Le Fèvre et al. 2000; Patton et al. 2000, 2002; Conselice et al. 2003; Xu et al. 2004; Lin et al. 2004; Bundy et al. 2004; Conselice et al. 2005; Bell et al. 2006b), but the observational uncertainty is large. Moreover, the few observational studies of the distribution of quasar host luminosities (Bahcall et al. 1997; McLure et al. 1999; Falomo et al. 2001; Hamilton et al. 2002; Jahnke & Wisotzki 2003; Dunlop et al. 2003; Floyd et al. 2004; Vanden Berk et al. 2006) have not yet determined if this distribution is expected (as a subset of the merging galaxy population), or whether it requires modes of quasar fueling aside from mergers of systems having reservoirs of cold gas. Some observations (Straughn et al. 2006) and theoretical analyses (Hopkins et al. 2005a) suggest that the stages most likely to be identified as mergers can be quite distinct from the merger-driven quasar phase, further complicating such comparisons.

Indirect evidence that mergers play a role in transforming galaxies also comes from studies of the stellar mass budget contained in morphologically or color-selected sub-populations as a function of redshift. For example, Borch et al. (2006) find that the stellar mass in red galaxies (known to be spheroid dominated) grows with time from $z \sim 1$ to the present. Furthermore, measurements of galaxy stellar mass functions separated by color or by morphology (Bundy et al. 2005a,b; Franceschini et al. 2006; Pannella et al. 2006) show that the "transition mass," above which red galaxies dominate the mass function, increases with redshift, following a general trend of "cosmic downsizing." As low-mass, red galaxies build up, the mass of the largest star-forming galaxies, although less well-constrained, decreases correspondingly, further supporting the view that star formation is "quenched" in these systems and that they move onto the red sequence (Bundy et al. 2005b). By comparing estimates of the transition or quenching mass to the characteristic masses of quasars (corresponding to the break in the observed quasar luminosity function) and merging galaxies, Hopkins et al. (2006d) have shown that these trace the same mass and evolve together over the range $0 < z \lesssim 3$, implying that these objects are linked. This connection motivates a detailed analysis to understand the relationship between the merger and quasar populations.

The contribution of mergers to the star formation density of the Universe is not well known, especially at high redshifts (e.g., Brinchmann et al. 1998; Menanteau et al. 2001, 2006; Bell et al. 2005). Traditional observational measurements which require morphological identification of star-forming galaxies are difficult to extend to these redshifts and are likely incomplete (Wolf et al. 2005), making particularly valuable any independent constraints that do not require direct morphological information, such as those from quasar populations. Even fewer estimates exist for the distribution of star formation rates in merging systems (e.g., Bell et al. 2005), and whether or not the measurements are consistent with gas-rich mergers passing through a starburst phase and building up the stellar mass observed in the elliptical galaxy population.

The significant uncertainties in the relation of elliptical galaxy, merger remnant, LIRG/ULIRG, merging (peculiar/interacting) galaxy, starburst, and quasar populations are related to the same underlying issue: Are the luminosity and mass distributions of quasars, quasar host galaxies, merging galaxies, starbursts, and ellipticals self-consistent? If the origin of red/elliptical galaxies primarily involves gas-rich mergers, with an intermediate starburst phase which is terminated by feedback from black hole growth dispersing gas, then these populations must track each other at all redshifts.

A long-standing obstacle to relating these populations has been the lack of theoretical models which incorporate the relevant physical processes. Large-scale cosmological simulations (e.g., Cen et al. 1994; Zhang et al. 1995; Hernquist et al. 1996; Katz et al. 1996a,b; Navarro et al. 1996; Croft et al. 1998, 1999, 2002; Davé et al. 1999; McDonald et al. 2000, 2006; Hui et al. 2001; Viel et al. 2003, 2004) and semi-analytic models (e.g., Kauffmann & Haehnelt 2000; Cole et al. 2000; Somerville et al. 2001; Volonteri et al. 2003; Wyithe & Loeb 2003; Granato et al. 2004; Somerville et al. 2004a; Baugh et al. 2005; Croton et al. 2006) have provided a framework for understanding the intergalactic medium and large-scale structure formation, but either do not resolve or do not follow the detailed effects of star formation, supernova feedback, black hole accretion and feedback, and dust obscuration, which are critical for inferring the relation between e.g. quasar and starburst populations and merger rates. Instead, these processes are described by idealized, tunable parameterizations rather than being modeled dynamically. Ideally, the prescriptions should be determined from physically motivated models, which have been tested against observations.

Recently, progress has been made in this direction by using high-resolution simulations of individual galaxies undergoing mergers that incorporate the effects of star formation and pressurization of multi-phase interstellar gas by supernova feedback (Springel & Hernquist 2003a) and feedback from black hole growth (Springel et al. 2005b). In this manner, Di Matteo et al. (2005) and Springel et al. (2005a,b) have shown that the gas inflows produced by gravitational torques during a merger (e.g. Barnes & Hernquist 1991, 1996) both trigger starbursts (e.g. Mihos & Hernquist 1994a, 1996) and fuel rapid black hole growth. During most of this phase, the black hole is heavily obscured (Hopkins et al. 2005a), but becomes briefly visible as a bright optical quasar when feedback expels the surrounding gas. As the gas is heated and dispersed, the accretion rate declines, leaving a dead quasar in an ordinary

galaxy. The self-regulated nature of this process explains observed correlations between black hole mass and properties of normal galaxies (Di Matteo et al. 2005), as well as the color distribution of ellipticals (Springel et al. 2005a).

Previously (Hopkins et al. 2005a-d, 2006a-c; Lidz et al. 2006), we have shown that this time evolution yields a self-consistent model for many observed properties of quasars, with no dependence on a particular prior cosmological distribution. In particular, the simulations imply a new description of quasar lifetimes where the lifetime of a given source depends on both the instantaneous *and* peak luminosities, so that for a given peak luminosity the lifetime *increases* at lower luminosities – i.e. quasars spend most of their lives in phases fainter than their peak luminosities. This leads to a different interpretation of the quasar luminosity function than is implied by idealized models of quasar lightcurves (in which quasars grow/decay in a step function or pure exponential manner); namely that the steep, bright end of the quasar luminosity function traces quasars accreting at high Eddington ratios near their peak luminosities, but the shallow, faint end is dominated by quasars with high peak luminosities but which are seen in less luminous states. The distribution of quasar birthrates as a function of their peak luminosities (final black hole masses), which is directly related to e.g. the gas-rich galaxy merger rate as a function of final galaxy mass, is *peaked* at a luminosity/mass corresponding to the break in the observed quasar luminosity function. Objects near the peak in this distribution dominate the observed faint-end quasar luminosity function in their fainter, below peak phases.

In Hopkins et al. (2006c), we used our modeling to predict the distribution of remnant elliptical galaxies formed in mergers. Because the spheroid stellar mass or velocity dispersion correlates with the final black hole mass in our simulations, we can use our model of quasar lifetimes and our determination of the birthrate of quasars as a function of their peak luminosity (final black hole mass) to infer the rate at which spheroids with given properties are formed in mergers as a function of e.g. mass, velocity dispersion, size, and redshift. In this manner, we reproduce spheroid mass, luminosity, and velocity dispersion functions, age distributions, mass-radius and luminosity-size relations, mass-to-light ratios, color-magnitude relations, and distributions of young (blue) spheroids at redshifts $z = 0-6$. The co-evolution of star formation, black hole growth, and obscuration is a key element in this analysis, and corresponding predictions made either neglecting the role of black hole feedback in terminating star formation or by modeling the quasar lightcurve in an idealized manner are inaccurate.

In principle, the merger hypothesis provides a framework for describing the co-formation of quasars and spheroids that reproduces a wide range of observations. To investigate this further, here we examine the statistics and properties of merging systems. In particular, we use our earlier modeling to study the implied relation between the quasar luminosity function (QLF), merging galaxy luminosity function (MGLF), quasar host galaxy luminosity function (HGLF), distribution of star formation rates in mergers (star formation rate function; SFRF), and the cumulative merger rates and star formation rate density triggered by mergers.

In § 2, we describe our simulations, and in § 3 we use them to determine the evolution of near-IR and optical/UV luminosities (§ 3.1), colors (§ 3.2), and star formation rates (§ 3.3) during mergers, as a function of host galaxy properties. In § 4 we describe our methodology for mapping between various distributions (§ 4.1), and discuss the impact and importance of possible systematic effects (§ 4.2). In § 5 we use our modeling to predict the quasar luminosity function from the observed merging galaxy function (at the same redshift), and vice versa (§ 5.1), in both *K*-band and the optical/UV. We use this to predict the underlying birthrate of spheroids/quasars with a given final mass/peak luminosity, and compare this with the observed merger mass functions (§ 5.2). Likewise, we use this to predict the distribution of star formation rates in mergers, independently from the observed quasar and merger luminosity functions, and compare with the observed star formation rate functions (§ 5.3). In § 6, we use the observed evolution in the quasar luminosity function to predict the evolution of the merging galaxy luminosity function and star formation rate function, as well as integrated quantities such as the luminosity, mass, and star formation rate densities in mergers, at redshifts $z = 0-6$. In § 7 we consider the relation between the MGLF and HGLF, predicting the quasar host galaxy luminosity function, the joint distribution of observed quasar and quasar host galaxy luminosities, and their co-evolution. Finally, in § 8, we summarize our results and discuss their implications for the merger hypothesis, various theoretical models, and future observations.

Our approach is described in detail in § 2-4, but readers interested in the main results may wish to skip to § 5 or § 7, where we compare and test the relation between various stages and measures of merger-driven activity, and § 6, which uses these relations to predict evolution of these measures with redshift.

Throughout, we adopt a $\Omega_M = 0.3$, $\Omega_\Lambda = 0.7$, $H_0 = 70\,\mathrm{km\,s^{-1}\,Mpc^{-1}}$ cosmology. All magnitudes are Vega magnitudes, unless otherwise stated.

2. THE SIMULATIONS

Our merger simulations were performed with the parallel TreeSPH code GADGET-2 (Springel 2005), based on a fully conservative formulation (Springel & Hernquist 2002) of smoothed particle hydrodynamics (SPH), which conserves energy and entropy simultaneously even when smoothing lengths evolve adaptively (see e.g., Hernquist 1993b, O'Shea et al. 2005). Our simulations account for radiative cooling, heating by a UV background (as in Katz et al. 1996, Davé et al. 1999), and incorporate a sub-resolution model of a multiphase interstellar medium (ISM) to describe star formation and supernova feedback (Springel & Hernquist 2003a). Feedback from supernovae is captured in this sub-resolution model through an effective equation of state for star-forming gas, enabling us to stably evolve disks with arbitrary gas fractions (see, e.g. Springel et al. 2005b; Springel & Hernquist 2005; Robertson et al. 2004, 2005). This is described by the parameter $q_{\rm EOS}$, which ranges from $q_{\rm EOS} = 0$ for an isothermal gas with effective temperature of 10^4 K, to $q_{\rm EOS} = 1$ for our full multiphase model with an effective temperature $\sim 10^5$ K.

Supermassive black holes are represented by "sink" particles that accrete gas at a rate $\dot{M}$ estimated from the local gas density and sound speed using an Eddington-limited prescription based on Bondi-Hoyle-Lyttleton accretion theory. The bolometric luminosity of the black hole is taken to be $L_{\rm bol} = \epsilon_r \dot{M} c^2$, where $\epsilon_r = 0.1$ is the radiative efficiency. We assume that a small fraction (typically $\approx 5\%$) of $L_{\rm bol}$ couples dynamically to the surrounding gas, and that this feedback is injected into the gas as thermal energy, weighted by the SPH smoothing kernel. This fraction is a free parameter, which we determine as in Di Matteo et al. (2005) by matching the

observed $M_{\rm BH}-\sigma$ relation. For now, we do not resolve the small-scale dynamics of the gas in the immediate vicinity of the black hole, but assume that the time-averaged accretion rate can be estimated from the gas properties on the scale of our spatial resolution (roughly $\approx 20\,$pc, in the best cases).

The progenitor galaxy models are described in Springel et al. (2005b), and we review their properties here. For each simulation, we generate two stable, isolated disk galaxies, each with an extended dark matter halo with a Hernquist (1990) profile, motivated by cosmological simulations (e.g. Navarro et al. 1996; Busha et al. 2005), an exponential disk of gas and stars, and (optionally) a bulge. The galaxies have total masses $M_{\rm vir}=V_{\rm vir}^3/(10GH_0)$ for $z=0$, with the baryonic disk having a mass fraction $m_{\rm d}=0.041$, the bulge (when present) having $m_{\rm b}=0.0136$, and the rest of the mass in dark matter. The dark matter halos are assigned a concentration parameter scaled as in Robertson et al. (2006b) appropriately for the galaxy mass and redshift following Bullock et al. (2001). The disk scale-length is computed based on an assumed spin parameter $\lambda=0.033$, chosen to be near the mode in the λ distribution measured in simulations (Vitvitska et al. 2002), and the scale-length of the bulge is set to 0.2 times this.

Typically, each galaxy initially consists of 168000 dark matter halo particles, 8000 bulge particles (when present), 40000 gas and 40000 stellar disk particles, and one BH particle. We vary the numerical resolution, with many simulations using twice, and a subset up to 128 times, as many particles. We choose the initial seed mass of the black hole either in accord with the observed $M_{\rm BH}$-σ relation or to be sufficiently small that its presence will not have an immediate dynamical effect, but we have varied the seed mass to identify any systematic dependencies. Given the particle numbers employed, the dark matter, gas, and star particles are all of roughly equal mass, and central cusps in the dark matter and bulge are reasonably well resolved (see Figure 2 in Springel et al. 2005b).

Our fitted quasar lifetimes and galaxy scaling relations are derived from a series of several hundred simulations of colliding galaxies, described in detail in Robertson et al. (2006a,b) and Hopkins et al. (2006b). We vary the numerical resolution, the orbit of the encounter (disk inclinations, pericenter separation), the masses and structural properties of the merging galaxies, initial gas fractions, halo concentrations, the parameters describing star formation and feedback from supernovae and black hole growth, and initial black hole masses.

The progenitor galaxies have virial velocities $V_{\rm vir}=80,113,160,226,320,$ and $500\,{\rm km\,s^{-1}}$, and redshifts $z=0,2,3,$ and 6, and our simulations span a range in final black hole mass $M_{\rm BH}\sim 10^5-10^{10}\,M_\odot$. The extensive range of conditions probed provides a large dynamic range, with final spheroid masses spanning $M_*\sim 10^8-10^{13}\,M_\odot$, covering essentially the entire range of the observations we consider at all redshifts, and allows us to identify any systematic dependencies in our models. We consider initial disk gas fractions (by mass) of $f_{\rm gas}=0.2,\ 0.4,\ 0.8,$ and 1.0 for several choices of virial velocities, redshifts, and ISM equations of state. The results described in this paper are based primarily on simulations of equal-mass mergers; however, by examining a small set of simulations of unequal mass mergers, we find that the behavior does not change dramatically for mass ratios down to about 1:3 or 1:4. This range is appropriate to the observations of merging galaxies used in this paper, which are restricted to 'major' merger events.

3. LUMINOSITIES, COLORS, AND STAR FORMATION RATES OF MERGERS

3.1. *Host Galaxy Luminosities*

To de-convolve the observed pair or merging galaxy luminosity function (MGLF) and infer a merger rate as a function of galaxy stellar mass, we must first describe the starburst lightcurves. In the simulations, star formation is tracked self-consistently, with stellar ages and stellar metallicities determined directly from the star-forming gas, which itself is enriched by star formation. We generally assume that pre-existing stars (i.e. initial bulge or disk stars when the gas fraction is less than unity) were formed with a constant star formation rate prior to the starting point of the simulation, with metal enrichment calculated self-consistently from the initial primordial gas. Considering instead exponentially declining star formation rates ("τ-models") or late-type star formation histories fitted from observations (e.g., Kauffmann et al. 2003b; Hammer et al. 2005) makes relatively little difference, and in any case stars formed over the course of the simulations usually dominate the observed luminosity. From the predicted ages and metallicities of the stars in our simulations, we use the stellar population synthesis models of Bruzual & Charlot (2003) assuming a Salpeter (1955) initial mass function, to measure the luminosity in a given band.

We determine attenuation in the manner described in Hopkins et al. (2005a, 2006b). Briefly, we calculate the column density along ~ 1000 lines-of-sight to each simulation stellar particle at each time, using the SPH formalism and multiphase ISM equation of state of the simulations (Springel & Hernquist 2003a) to determine the density, metallicity, and ionization state of gas in the "warm/hot" ISM through which the majority of sightlines will pass (i.e. neglecting mass collapsed in cold clouds). We adopt a gas-to-dust ratio scaled by metallicity (e.g., Bouchet et al. 1985) and normalized to that of the Milky Way, $A_B/N_{\rm H\,I}=8.47\,(Z/0.02)\times 10^{-22}\,{\rm cm^2}$, and a Small Magellanic Cloud-like reddening curve (as suggested by observations for the host galaxies of quasars, e.g. Hopkins et al. 2004, Ellison et al. 2005, although the 280 nm cross-section is decreased by only 6% if we instead assume a Milky Way-like reddening curve) with the form from Pei (1992), to attenuate the intrinsic spectrum of each stellar particle. We do not perform a full radiative transfer calculation, and therefore do not model scattering or re-processing of radiation by dust in the infrared. However, we compare the column densities to quasars calculated by variations of this method in Hopkins et al. (2005b) (see their Figures 1, 5, & 6) and find that typical uncertainties are a factor $\sim 2-3$ in $N_{\rm H}$, generally smaller than the variation across different simulations and viewing angles. Furthermore, we find below that our results for the visible (attenuated) luminosities agree well with those expected from the calculations in Jonsson et al. (2006) which employ a complete Monte Carlo radiative transfer model.

This modeling effectively captures obscuration by gas and dust in the "typical" ISM, but does not, however, directly resolve individual molecular clouds or e.g. dense nuclear concentrations of molecular gas, which have important effects on the mid and far-IR spectra of the nuclear starbursts of LIRGs and ULIRGs. These effects are unimportant in our analysis, for several reasons. First, the duration of the starburst is short ($\sim 10^8\,$yr) compared to the total time during which a merger will be identified ($\sim 10^9\,$yr), and the fraction of the total stellar mass formed therein is small. Most of the time the merger

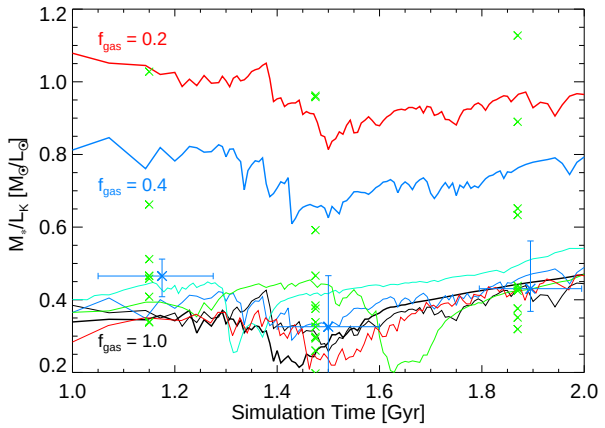

FIG. 1.— Ratio of total stellar mass to total K-band luminosity as a function of time in three representative simulations with gas fractions $f_{\rm gas} = 0.2,\ 0.4,\ 1.0$ as labeled (thick lines). For $f_{\rm gas} = 1.0$, several simulations with $V_{\rm vir} = 80-320\,{\rm km\,s^{-1}}$ and $q_{\rm EOS} = 0.25-1$ are shown (thin lines). Green points show observed ULIRGs (expected to correspond to high-$f_{\rm gas}$ mergers), with blue points showing the median and interquartile range, from the observed merging ULIRG pair sample of Dasyra et al. (2006) ($t \sim 1.2\,$Gyr; horizontal error roughly illustrates the times corresponding to observed separations), the late-stage ULIRG sample of Tacconi et al. (2002) ($t \sim 1.5\,$Gyr), and the merger-remnant LIRG/ULIRG sample of Rothberg & Joseph (2004) ($t \sim 1.9\,$Gyr). The K-band mass-to-light ratio depends weakly on gas fraction in a systematic manner, but not on other varied merger properties, and agrees well with typical observed values.

will be a weakly-interacting pair or post-merger remnant, so corrections to luminosity or mass functions will in any case be small, $\lesssim 10\%$. Moreover, surveys identifying mergers by pair counts or tidal features with which we compare generally do not include the heavily obscured starburst stage.

Second, we explicitly confine ourselves to consider the near-IR through near-UV, where the effects of these obscuration mechanisms are minimized. For typical ULIRGs, central luminosities can be heavily extinguished with $A_\lambda \sim 50$ even in K-band; but as a consequence the integrated luminosity is dominated by stars in more extended regions, which are obscured by the relatively quiescent ISM with a much lower effective total or "screen" extinction of ~ 0.7 magnitudes (e.g., Lonsdale et al. 2006), similar to that in our simulations. Third, re-radiation is relatively unimportant in the bands we consider, and at the point of the nuclear starburst, even the typical ISM densities are sufficient to render the most dense regions optically thick. At such a point, the obscuration mechanism and the "degree" of optical thickness are unimportant. Finally, we have compared with full radiative transfer models in the far-IR through UV, including dust heating and considering different sub-resolution models for the detailed clumping of molecular gas (Narayanan et al. 2006; Chakrabarti et al. 2006), and find little change in the total luminosity in the bands we consider here, even during peak starburst stages.

3.1.1. *K-band Luminosities*

We first consider the K-band galaxy luminosity in mergers. In each simulation, we calculate and plot the total stellar mass divided by total K-band luminosity as a function of time. Figure 1 shows the result for several representative cases, some with identical virial velocities, but a varying gas fraction, and others with the same $f_{\rm gas}$, but either different $V_{\rm vir}$ or $q_{\rm EOS}$. There is no clear systematic difference in $M/L_{\rm K}$ at fixed gas fraction (we have also varied e.g. initial black hole mass, presence or absence of initial bulges, and orbital parameters and find the same). However, there is a systematic dependence on the gas fraction, so that $M/L_{\rm K}$ is somewhat lower for high-$f_{\rm gas}$ systems which are dominated by younger stellar populations.

We can estimate this effect quantitatively as a function of $f_{\rm gas}$ with a model in which a galaxy of total final stellar mass $M_{*,\,\rm tot}$ forms a fraction $f_{\rm gas}$ of its mass in the merger (i.e. assuming the limit of efficient conversion of gas to stars) with mass-to-light ratio $(M/L_{\rm K})_{\rm new}$, and the remaining mass coming from an older population with $(M/L_{\rm K})_{\rm old}$. This gives

$$\frac{M}{L_{\rm K}} = \frac{(M/L_{\rm K})_{\rm new}}{f_{\rm gas} + (1-f_{\rm gas})\,\frac{(M/L_{\rm K})_{\rm new}}{(M/L_{\rm K})_{\rm old}}}. \quad (1)$$

Fitting to the mean $M/L_{\rm K}$ in our mergers as a function of $f_{\rm gas}$ gives $(M/L_{\rm K})_{\rm new} \approx 0.4$ and $(M/L_{\rm K})_{\rm old} \approx 1.4$, corresponding to stellar populations with mean ages ~ 0.5 and $5\,$Gyr, respectively, reasonable values for observed mergers. This equation gives the mean $M/L_{\rm K}$ accurate to $\sim 10-20\%$; i.e. comparable to the scatter in $M/L_{\rm K}$ in a given merger and across mergers with varied parameters (but similar gas fractions). Note that the dependence is fairly weak, as a factor of 2 change in gas fraction (e.g. $f_{\rm gas} = 0.1 \rightarrow 0.2$ or $f_{\rm gas} = 0.2 \rightarrow 0.4$) results in only a $\sim 20\%$ change in $M/L_{\rm K}$, generally smaller than the relevant observational uncertainties.

The K-band total mass-to-light ratio is also relatively constant with time in a merger. In part, this owes to the weak dependence of $M/L_{\rm K}$ on stellar population age and the continuous star formation throughout the merger. For example, given a constant star formation rate (SFR) beginning at $t = 0$, and ignoring older stars (i.e. roughly the $f_{\rm gas} = 1$ case), we expect $M/L_{\rm K}$ to increase by only $\sim 40\%$ from $t = 1\,$Gyr to $t = 2\,$Gyr, as in Figure 1. Moreover, as seen in simulations (Hopkins et al. 2006b; Jonsson et al. 2006) and observations of local ULIRGs such as Arp 200 (Doyon et al. 1994; Lonsdale et al. 2006), increased densities in the merger give rise to both elevated star formation but also enhanced obscuration, resulting in a flat observed host galaxy luminosity during these times.

Unfortunately, without a large sample of mergers or a reliable means to determine the exact merger stage or pre-merger $f_{\rm gas}$, comparing our predicted $M/L_{\rm K}$ as a function of time with observations is not possible, but we can check for consistency. In Figure 1, we plot $M/L_{\rm K}$ of observed merging ULIRG pairs with masses determined from dynamical measurements in Dasyra et al. (2006) at $t \sim 1.2\,$Gyr, corresponding roughly to the stage at which the merging nuclear pair separations are comparable. Green crosses show individual objects, blue points the median and interquartile range, with horizontal errors heuristically corresponding to times in which a given merger would appear in the observed sample. At $t \sim 1.5\,$Gyr we show the same, for the late-stage ULIRG sample of Tacconi et al. (2002), and at $t \sim 1.9\,$Gyr, for the post-merger LIRG/ULIRG sub-sample of Rothberg & Joseph (2004). At each stage, the typical values and scatter in $M/L_{\rm K}$ correspond well with that expected, especially given the additional scatter in observed samples from measurement errors and a range in observed $f_{\rm gas}$ (note that the observed samples are all selected to be ULIRGs, so we expect they will correspond to the most gas-rich mergers we simulate). The later-stage (non-LIRG) merger remnant sample of Rothberg & Joseph (2004) forms a continuum in $M/L_{\rm K}$ from these values to those typical of old ellipticals $M/L_{\rm K} \sim 1.4$, presumably as these populations age and redden.

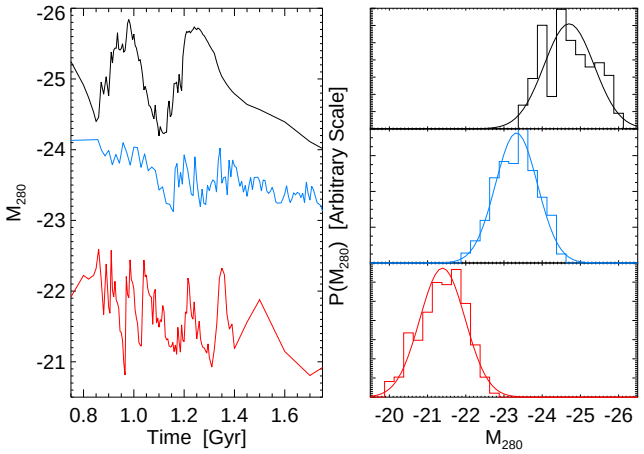

FIG. 2.— Left: Median observed (attenuated) magnitude at 280 nm as a function of time during the peak merger stages from three representative simulations with $V_{\rm vir}$ = 80, 160, and 320 km s^{-1} (red, blue, and black, respectively). Right: Distribution of observed magnitudes (each weighted by the amount of time across all sightlines that the galaxy is observed at a given M_{280}) for each simulation (histograms of corresponding colors), with best-fit Gaussians (smooth curves). The distribution of optical/UV luminosities is relatively constant throughout the merger, with enhanced star formation and obscuration offsetting one another, and is well-fitted by a Gaussian PDF.

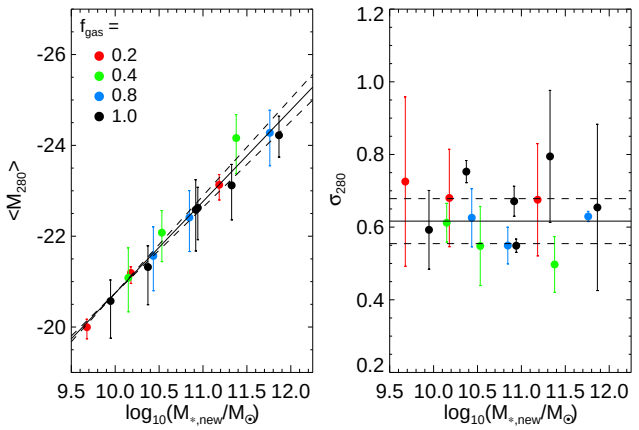

FIG. 3.— Left: Mean observed 280 nm magnitude over the course of a merger for simulations with $V_{\rm vir}$ = 80−320 km s^{-1} and gas fractions as labeled (circles), as a function of the mass of stars formed during the merger, $M_{*,\rm new}$. Vertical errors show the range allowing for a factor of 3 uncertainty in the calculated column density. Solid line shows the best-fit power law, dashed lines the 1σ range of this fit. Right: Dispersion in 280 nm magnitude over the course of a merger, for the same simulations (symbols as in left panel). Solid line shows the best-fit constant σ_{280} and dashed lines the 1σ range. The PDF for observing a merger at a given luminosity has a constant shape and width, with the mean optical/UV luminosity scaling with the mass of stars forming in the merger.

3.1.2. *280 nm Luminosities*

Next, we examine a synthetic UV band centered at 280 nm, with a 40 nm width, for comparison with the results of Wolf et al. (2005) from the GEMS and GOODS surveys. This band is normalized to the solar luminosity in the 280/40 passband, which is $M_{\odot,280}$ = 6.66 in Vega units or $L_{\odot,280}$ = 2.56×10^{10} W/Hz. Here, we use the Starburst99 population synthesis models (Leitherer et al. 1999) to calculate the UV spectra of the stellar particles. Figure 2 shows the outcome of this calculation for three representative simulations, with $f_{\rm gas}$ = 1.0, $z_{\rm gal}$ = 0, $q_{\rm EOS}$ = 1.0, and varying $V_{\rm vir}$, as labeled. The median observed M_{280} as a function of time during the merger is shown for each simulation (left panel). Again, the effects of star formation and dust obscuration tend to offset one another, and the host galaxy luminosity varies within a factor $\lesssim 2$, i.e. within 1 magnitude, throughout the merger, even though the *intrinsic* (un-attenuated) UV luminosity can rise by a much larger factor.

We calculate (Figure 2, right panel) the probability of observing a given M_{280}, i.e. the total time a given M_{280} is visible integrated over all sightlines and over the duration of the merger. The results are shown as histograms of the corresponding color for each merger in the left panel (with the best-fit Gaussian). In each case, the PDFs have a well-defined peak and narrow ($\sim$ 0.6 mag) width in M_{280}, emphasizing that the light curves are quite flat. The Gaussian fits allow us to statistically characterize the lightcurves of our simulations with a mean M_{280} and rms dispersion about this mean, σ_{280}.

In Figure 3, we quantify the dependence of the mean observed 280 nm luminosity on host galaxy properties. We include a subset of our simulations with various values of $f_{\rm gas}$, as labeled, and for each, $V_{\rm vir}$ = 113, 160, and 320 km s^{-1} and $q_{\rm EOS}$ = 1.0. For $f_{\rm gas}$ = 1.0, we also calculate the results for $V_{\rm vir}$ = 80, 226 km s^{-1}, $q_{\rm EOS}$ = 1.0 and for $V_{\rm vir}$ = 160 km s^{-1}, $q_{\rm EOS}$ = 0.25, to demonstrate that these variations do not alter our conclusions. We plot the mean M_{280} and rms dispersion σ_{280} for each simulation. The vertical error bars show the range resulting from a systematic increase or decrease in our estimated column densities (roughly parameterizing the maximal uncertainty for our calculation of $N_{\rm H}$ from Hopkins et al. 2005b). We expect the UV luminosity will be dominated by young stars, and therefore show the mean M_{280} as a function of the mass of stars formed during the merger, $M_{*,\rm new}$. Unsurprisingly, the two are well correlated, and the scaling does not depend on gas fraction, virial velocity, or ISM gas equation of state. Fitting a relation of the form

$$M_{280} = M_{280,0} + \alpha\,\log_{10}\left(\frac{M_{*,\rm new}}{10^{10}\,M_{\odot}}\right) \quad (2)$$

gives a best fit $M_{280,0} = -20.7\pm0.1$, $\alpha = -2.01\pm0.13$, shown as a solid black line. In terms of L_{280},

$$L_{280} = L_{280,0}\left(\frac{M_{*,\rm new}}{10^{10}\,M_{\odot}}\right)^{0.80\pm0.05}, \quad (3)$$

where $L_{280,0} = 5.06\pm0.45\times10^{10}\,L_{\odot,280}$. The dispersion σ_{280} has no significant dependence on stellar or black hole mass, gas fraction, or other host properties. The solid line (dashed lines) shows the best fit ($\pm1\sigma$) mean $\sigma_{280} = 0.62\pm0.06$ (0.25 dex in L_{280}). There are limited observations to compare against, but these values are consistent with the colors and inferred star formation properties in e.g. Bell et al. (2006a).

The scaling of M_{280} with host properties can be understood in terms of a model assuming efficient conversion of gas to stars. Given that general trends in star formation rate as a function of time are qualitatively similar regardless of the total number of stars formed, the intrinsic (un-attenuated) UV luminosity (henceforth $L_{\rm int}$) should scale proportionally with the mass of new stars formed, $L_{\rm int} = \langle M/L_{280}\rangle^{-1} M_{*,\rm new}$, where $\langle M/L_{280}\rangle$ is an effective mass-to-light ratio depending on the star formation history. The timescale of $\sim$ 1 Gyr during which the galaxies will be visible as a merger, or alternatively the fit to $M/L_{\rm K}$ from our simulations or observations (Tacconi et al. 2002), imply $\langle M/L_{280}\rangle \approx 0.08\,M_{\odot}/L_{\odot,280}$, corresponding to a population with an age of 0.5 Gyr.

However, the observed luminosity does not scale as steeply as $L_{\rm int} \propto M_{*,\rm new}$, owing to higher attenuation as the gas mass increases. Jonsson et al. (2006) consider lightcurves of merging galaxies using a smaller set of simulations (without black holes), but with a full Monte Carlo radiative transfer code, and demonstrate that it is reasonable to assume that the newly-formed stars and star-forming gas (which produces most of the obscuration) are well-mixed, giving an observed luminosity $L_{280} = L_{\rm int}\,\tau^{-1}\,(1-e^{-\tau})$ (e.g., Calzetti et al. 1994), where τ is an effective mean optical depth. From their fits to the attenuation in bolometric, SDSS *u*-band, and GALEX NUV luminosities we estimate $\tau \approx \tau_0\,(M_g/10^{11}\,M_\odot)^{0.16}$, where $\tau_0 \approx 2-3$ and $M_g \approx M_{*,\rm new}$ is the gas mass, which they show can be roughly understood in terms of how both the SFR and obscuration scale with local gas density. Given $\tau \gtrsim 1$, the attenuation goes as $L_{280} \propto \tau^{-1}$, and we can combine the scalings to obtain the expected relation

$$L_{280} \approx 5.8-8.7\times10^{10}\,L_{\odot,\,280}\left(\frac{M_{*,\rm new}}{10^{10}\,M_\odot}\right)^{0.84}, \qquad (4)$$

in good agreement with the scaling of L_{280} measured in the simulations. That these scalings agree emphasizes that contributions to the observed L_{280} from older stellar populations are relatively small ($\lesssim 30\%$). Furthermore, this suggests that our results using just the calculated column densities (i.e. ignoring scattering processes) would not be significantly changed by a more sophisticated treatment of radiative transfer.

Finally, the conversion of gas to stars in mergers is efficient, i.e. $M_{*,\rm new} \approx f_{\rm gas} M_{*,\rm tot} = f_{\rm gas} M_*$ (true to $\lesssim 10\%$ over $f_{\rm gas} \sim 0.2-1.0$), where for simplicity we subsequently denote the final, total stellar spheroid mass as $M_* = M_{*,\rm tot}$. Our calculations then describe the statistics of *K*-band and 280 nm luminosities in mergers as a function of $f_{\rm gas}$ and M_*, with no systematic dependence (quantified in this manner) on the other parameters we have varied.

3.1.3. *Other Optical and Near-IR Luminosities*

For future reference, we perform the above set of calculations in several different wavebands (280 nm, U, B, V, R, I, J, H, K, and SDSS u, g, r, i, z), calculating for each the equivalent of Equation (2), i.e. the best-fit relation between the median magnitude in the given band ($M_{\rm BAND}$) and total stellar mass formed in the merger ($M_{*,\rm new}$), as well as the dispersion in a given merger about the expected median magnitude ($\sigma_{\rm BAND}$). The results are shown in Table 1. We also consider fits to $M_{\rm BAND}$ as a function of final black hole mass $M_{\rm BH}$ or total final stellar mass $M_{*,\rm tot}$ instead of $M_{*,\rm new}$. For each, we show the resulting χ^2/ν, which measures the goodness-of-fit. Note that a small χ^2/ν implies small scatter about the fitted relation, but does not imply that there is no systematic dependence on certain external variables.

For example, in the optical/UV, the correlation between $M_{\rm BAND}$ and $M_{*,\rm new}$ or $M_{*,\rm tot}$ is comparable, but as demonstrated above, there is a systematic dependence on $f_{\rm gas}$ if $M_{\rm BAND}$ is quantified as a function of $M_{*,\rm tot}$ (brighter optical/UV at higher gas fractions). Note that $\sigma_{\rm BAND}$ also quantifies the degree to which it is appropriate to assume that the luminosity in the given band over the course of the merger is constant (a poor approximation to the bolometric luminosity, but a surprisingly good one in the bands we measure). These should be of particular use in comparing cosmological simulations and semi-analytic models with observed merger populations, and enable future observations of merger luminosity functions to easily estimate their contributions to remnant spheroid and quasar populations.

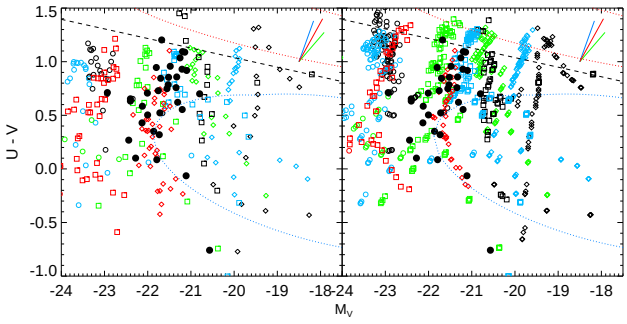

FIG. 4.— Color-magnitude relation at ~ 100 random times and sightlines during each of several merger simulations with $V_{\rm vir}$ = 116, 160, 320 km s^{-1} (diamonds, squares, and open circles, respectively), $f_{\rm gas}$ = 0.2, 0.4, 0.8, 1.0 (black, blue, green, and red, respectively), $z_{\rm gal} = 0$, $q_{\rm EOS} = 1.0$. The left panel neglects dust attenuation, the right panel includes this effect. In each, solid lines show the impact of increasing metallicity (from $0.1\,Z_\odot - Z_\odot$; blue), age (from 0.5 – 1 Gyr; green), and column density (from $N_{\rm H} = 0-10^{21}$ cm^{-2}; red). Filled black circles show local ULIRGs from Surace et al. (2000) and Arribas et al. (2004), K-corrected following Bell et al. (2005). For comparison, dotted contours (roughly) show the local red sequence (red) and blue cloud (blue), with the "valley" separating the two from Bell et al. (2005) (dashed). The color-magnitude distribution of the simulations is similar to that observed, with roughly equal contributions from stellar population effects and variations in column densities.

3.2. *Colors and Color-Magnitude Relations*

In Figure 4, we plot the $(U-V)$ vs. M_V color-magnitude relation for each of several representative simulations with different virial velocities and gas fractions $f_{\rm gas} = 0.2-1.0$, fixing $z_{\rm gal}$ and $q_{\rm EOS}$. For each simulation, we consider ~ 100 randomly selected points in time at which the merger is "observed" during the ~ 2 Gyr during which the system shows evidence of merging, and at each point in time consider a random sightline (uniformly sampling the unit sphere). In the left panel, we neglect the effects of dust attenuation. We illustrate the age/metallicity/obscuration degeneracy with the solid lines in the upper right, which demonstrate how a point in the color-magnitude space is moved (from the point of origin of the three lines) with increasing mean stellar age, metallicity, or column density.

The wide scatter in $(U-V)$ colors in both panels demonstrates that the effects of different mean stellar ages and metallicities contribute strongly to the scatter in the color-magnitude relation. The evolution is difficult to disentangle, as increasing age and metallicity in later stages generally redden the merger, but the final merger is associated with a starburst which briefly reduces the mean (luminosity-weighted) age. Differential extinction actually marginally decreases the color spread, as intrinsically blue periods (i.e. times of peak star formation) tend to be heavily dust-reddened, whereas intrinsically red periods (e.g. post-merger stages) are only weakly affected. Although the scatter in $(U-V)$ may derive largely from stellar population effects, this does not imply that extinction is unimportant. The mean effective total or "screen" reddening is $\sim 0.2-0.5$ magnitudes and during the peak starburst phase this rises to $\gtrsim 1-2$ mag, similar to that observed (e.g., Genzel et al. 1998). (Note, however, that the spatially resolved extinction can be much greater in the very central regions during these phases.) Extinction also reddens objects out of the bright blue ($M_V \lesssim -21$, $(U-V) \lesssim 0$) region

of the color-magnitude diagram (quantitatively, the fraction of points in this region drops from $\sim 10\%$ to $\sim 1\%$ when attenuation is included). The faint, red region is not especially heavily populated, which is of interest for optically or UV-selected samples, especially at high redshift, which may not be sensitive to faint red mergers (see e.g. Bell et al. 2005; Wolf et al. 2005, for further discussion). We emphasize though that there is no real color-magnitude "relation," and thus any physical inferences from the observed color-magnitude distribution should be considered with caution.

We plot for comparison (filled circles) the locations of local ULIRGs from Surace et al. (2000) and Arribas et al. (2004) following Bell et al. (2005). Quantitative comparison is difficult, but the observed and simulated loci are similar, especially compared to the blue cloud and red sequence on which the progenitor and remnant galaxies lie, respectively (see Springel et al. 2005a). We have also compared the $(280-V)$, $(U-B)$, $(B-R)$, and $(R-K)$ colors with observed color-magnitude distributions of the $z\approx 0.7$ interacting sample of Bell et al. (2005) and Wolf et al. (2005), and the morphologically irregular starburst sample of de Mello et al. (2006), as well as the GEMS host galaxy sample of active galactic nuclei (AGN) of Sánchez et al. (2004) (see e.g. Figure 7 of Bell et al. 2005), and find similar broad agreement. The substantial scatter in metallicities during mergers is also comparable to that in Rothberg & Joseph (2006), and rough trends in obscuration and metallicity with stellar mass or luminosity in the star-forming stages are similar to those observed (Burstein et al. 1988; Worthey et al. 1992; Faber et al. 1995; Jørgensen 1997; Kuntschner 2000).

3.3. *The Star Formation Rate Distribution in Individual Mergers*

Because the star formation rate is far from constant during a merger, sharply peaking during the starburst phase and falling off exponentially afterwards, with smaller peaks in earlier stages, a given merger will not necessarily be observed near a single characteristic SFR (as with e.g. the luminosities calculated above). We can, however, consider the time a given simulation spends in a given interval in SFR (i.e. the SFR-dependent "lifetime" of the merger) and use this to quantify the distribution of SFRs in mergers. In detail, the time-behavior of the SFR, $\dot{M}_*$, is somewhat chaotic, with a systematic dependence on virial velocity, ISM gas equation of state, galaxy gas fractions, and merging galaxy mass ratio. However, when rescaled in terms of the *total* mass of new stars formed during the merger, $M_{*,\rm new}$, the critical statistical property of the SFR distribution, namely the time spent by a given simulation in a given interval in $\dot{M}_*$, is essentially unaffected by these systematics.

In Figure 5, we determine the integrated time spent by each of ~ 100 simulations above a given SFR (from $\dot{M}_*\sim 10^{-4}-10^{3}\,{\rm M_\odot\,yr^{-1}}$), as a function of that SFR, $\dot{M}_*$. We then rescale the SFR by dividing out a characteristic SFR, $M_{*,\rm new}/t_*$, i.e. the total new stellar mass formed during the merger divided by some characteristic starburst timescale. For now, t_* is arbitrary (we choose $t_*=0.65\,$Gyr, for the reasons below). We plot, for each simulation, the time spent above a given dimensionless SFR ($\dot{M}_*/(M_{*,\rm new}/t_*)$). We show this for the simulations in bins of $\log(M_{*,\rm new})$ from $M_{*,\rm new}\sim 10^{9}-10^{13}$. In each bin, different colored lines correspond to different initial conditions in the simulations, various combinations of $V_{\rm vir}=80-500\,{\rm km\,s^{-1}}$, $q_{\rm EOS}=0,\ 1$, $z_{\rm gal}=0,\ 2,\ 3,\ 6$, and

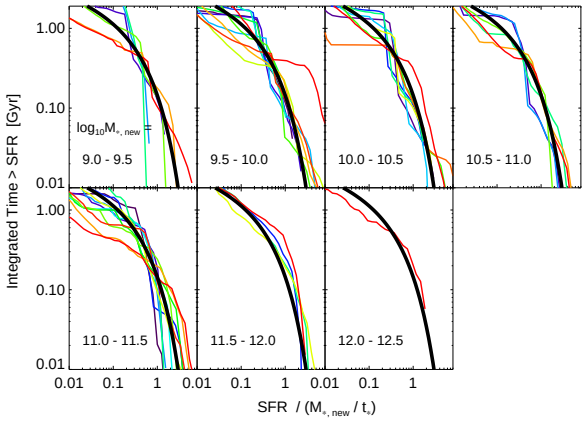

FIG. 5.— Integrated time above a given rescaled star formation rate $\dot{M}/(M_{*,\rm new}/t_*)$, where $M_{*,\rm new}$ is the mass of new stars formed during the merger and $t_*=0.65\,$Gyr is fitted. Results are shown for ~ 100 simulations, in bins of $M_{*,\rm new}$ as labeled. Different colors show simulations with different values of $V_{\rm vir}$, $f_{\rm gas}$, $q_{\rm EOS}$, $z_{\rm gal}$. The thick black line in each interval shows the fitted analytical approximation of Equation (5). Quantified in this manner, the PDF for observing a given merger at some instantaneous SFR is well-determined and independent of systematic effects from varied quantities in the simulations.

$f_{\rm gas}=0.2,\ 0.4,\ 0.8,\ 1.0$. Although there is significant scatter in the time spent above some SFR between different simulations, we find that once rescaled in this manner, there is no systematic dependence on any of the varied quantities.

We fit the "lifetime" at a given SFR in Figure 5 to an analytical function following Hopkins et al. (2006b),

$$\frac{{\rm d}t}{{\rm d}\log\dot{M}_*} = t_*\,\ln(10)\,\exp\left(-\frac{\dot{M}_*}{M_{*,\rm new}/t_*}\right), \qquad (5)$$

where $M_{*,\rm new}$ is the total stellar mass formed in the merger, t_* is a characteristic timescale, and the normalization $t_*\,\ln(10)$ is determined by the integral constraint

$$\int \dot{M}_*\,{\rm d}t = \int \dot{M}_*\,\frac{{\rm d}t}{{\rm d}\log\dot{M}_*}\,{\rm d}\log(\dot{M}_*) = M_{*,\rm new}. \qquad (6)$$

This gives a one-parameter function to describe the statistical properties of the SFR distribution in mergers.

Fitting to the simulations, we find a best-fit $t_*\approx 0.65\pm 0.10\,$Gyr, with no evidence for a strong dependence of t_* on $M_{*,\rm new}$ or other varied parameters. This is comparable to the star formation timescale implied by observations of starburst galaxies (Kennicutt 1998) and mean luminosity-weighted ages of merger stellar populations (Tacconi et al. 2002). We show the prediction of this fit as the thick black lines in each panel of Figure 5. The form of Equation (5) suggests an exponentially increasing/decreasing SFR into/out of the starburst peak. However, too much detail should not be read into the precise SFR as a function of time from these fits, as they both average over the entire merger and do not capture a systematic dependence such as the tendency of higher-mass systems to form a larger fraction of their stars prior to the final merger (Robertson et al. 2006a). As an aside, a similar functional form could be used to describe quiescent SFRs in exponentially declining "τ-models," but in this case would be characterized by a much lower typical SFR ($\sim f_{\rm gas}M_{\rm disk}/10\,$Gyr) and higher normalization $\sim\tau\ln 10$ (where $\tau\sim 4-8\,$Gyr is the SFR timescale in stable disks; e.g. Li et al. 2005, 2006).

4. METHODOLOGY: COMPARING MERGER AND QUASAR DISTRIBUTIONS

4.1. *Converting Between Merger, Quasar, and SFR Distributions*

If the merging galaxy luminosity function (MGLF) in a band ν is given by $\phi_{\rm gal}(L_\nu) \equiv {\rm d}\Phi/{\rm d}\log(L_\nu)$, then

$$\phi_{\rm gal}(L_\nu) = \int \frac{{\rm d}t}{{\rm d}\log(L_\nu)}\, \dot{n}(M_*)\, {\rm d}\log M_*, \quad (7)$$

where $\dot{n}(M_*) = {\rm d}n\,{\rm d}t^{-1}\,{\rm d}\log(M_*)^{-1}$ is the merger rate as a function of final stellar mass, and ${\rm d}t/{\rm d}\log(L_\nu)$ is the time the merger is visible in a logarithmic interval in L_ν. Because, as shown in § 3.1, the merging galaxy luminosity is quite flat in time, and the timescale over which merging galaxies are identifiable as such ($\sim 2\,$Gyr) does not depend strongly on the galaxy masses over the range of interest, we can use ${\rm d}t/{\rm d}\log(L_\nu) = P(L_\nu\,|\,M_*)\,t_{\rm merge}$, where $P(L_\nu\,|\,M_*)$ is the probability (calculated in § 3.1) of being observed in a logarithmic interval in L_ν over the merger timescale ($t_{\rm merge}$). The deconvolution of the MGLF, $\phi(L_\nu)$, with the PDF for observing a merger at a given luminosity $P(L_\nu\,|\,M_*)$ directly yields the merger mass function for a given luminosity function.

Having considered the observed properties of mergers with some final spheroid mass M_*, we can use the scalings between black hole mass and host galaxy velocity dispersion or stellar spheroid mass to relate each merger to an associated black hole. The relation between final (post-merger) black hole mass and total stellar mass in our simulations is

$$M_{\rm BH} \approx 0.001\,M_*, \quad (8)$$

(Di Matteo et al. 2005; Robertson et al. 2006b), with an approximately lognormal scatter of $\sim 0.3\,$dex, essentially identical to observational estimates from e.g. Marconi & Hunt (2003); Häring & Rix (2004) (accounting for the difference between virial and stellar mass). Knowing $M_{\rm BH}(M_*)$, we can convert $\dot{n}(M_*)$ to $\dot{n}(M_{\rm BH})$, the birthrate of quasars of a given relic mass in galaxy mergers,

$$\dot{n}(M_{\rm BH}) = \int P(M_{\rm BH}\,|\,M_*)\,\dot{n}(M_*)\,{\rm d}\log M_*\,. \quad (9)$$

We can then express the observed QLF in terms of $\dot{n}(M_{\rm BH})$ and the quasar lifetime as a function of luminosity (see Equation [10]), identical to the expression in Equation (7) but with M_* replaced by $M_{\rm BH}$.

Given a model for the quasar lifetime ${\rm d}t/{\rm d}\log(L_\nu)$, then, the QLF is determined. We generally consider two cases: first, a "feast or famine" or "light-bulb" model for the quasar lifetime, following what has generally been adopted in previous works (e.g., Small & Blandford 1992; Kauffmann & Haehnelt 2000; Haiman & Menou 2000; Wyithe & Loeb 2003; Volonteri et al. 2003; Haiman, Quataert, & Bower 2004). In one typical scenario of this type, the quasar turns on in a merger, accretes at constant Eddington ratio $\dot{m}$, and then either "turns off" or exponentially decays in luminosity (Haiman & Loeb 1998). The lightcurve is an exponential, $L \propto \exp(\pm t/t_Q)$, and the lifetime as a function of luminosity is trivial, ${\rm d}t/{\rm d}\log(L) = \ln 10\; t_Q = $ constant (for $L < L_{\rm peak}$), where t_Q is a free parameter. Assuming an even simpler description in which quasars "turn on" at fixed luminosity $L = L_{\rm peak}$ for a fixed t_Q, produces nearly identical results. Generally, t_Q is either adopted from observations (with the loose constraint $t_Q \sim 10^6 - 10^8\,$yr; see Martini 2004 for a review) or assumed to be the Salpeter (1964) time $t_S = 4.2\times10^7\,$yr (*e*-folding time at $\dot{m} = 1$ with radiative efficiency $\epsilon_r = 0.1$), but we allow it to vary to provide the best fit to the observed QLF.

In Hopkins et al. (2005a,b, 2006a,b), we compare these idealized scenarios to the light curves and lifetimes derived from our simulations and find that they provide a poor representation at any luminosity. The simulation lightcurves are complex, with multiple phases of activity, variability, and feedback-regulated decay, but their statistical nature can be described by simple forms (Hopkins et al. 2005b, 2006b). The key feature of the quasar lifetime not captured by more idealized models is that it *increases* with decreasing luminosity; i.e. a given quasar spends more time at luminosities below its peak than at its peak luminosity. In Hopkins et al. (2006b,c) we use our simulations to calculate the differential quasar lifetime, i.e. the time spent in a given logarithmic luminosity interval, and find it is well-fitted by a Schechter function,

$$\frac{{\rm d}t}{{\rm d}\log(L)} = t_Q \left(\frac{L}{L_Q^*}\right)^{-\alpha} \exp[-L/L_Q^*]. \quad (10)$$

Here, L_Q^* is proportional to the *peak* quasar luminosity $L_{\rm peak} \sim L_{\rm Edd}(M_{\rm BH})$, t_Q is a fixed constant ($t_Q = \frac{\ln 10}{\eta} t_S$ for $L_Q^* = \eta L_{\rm peak}$), and $\alpha \sim 0.5$ is weakly dependent on peak luminosity and is determined by the nearly scale-invariant "blowout" of gas as exponentially growing feedback from black hole growth heats the gas rapidly and it can no longer cool efficiently in a dynamical time (Hopkins et al. 2006a). The lifetime in Equation (10) is entirely determined by our simulations, and when quantified as a function of $L_{\rm peak}$ in this manner, the quasar lifetime shows no systematic dependence on host galaxy properties, merger parameters, initial black hole masses, ISM and gas equations of state and star formation models, or other varied parameters (see Hopkins et al. (2006b) for a detailed discussion and calculation).

Having quantified the luminosity dependent quasar or merger "lifetime" in a manner independent of the detailed initial conditions above, we can map between merger and quasar populations without requiring any cosmological priors on their distributions. Thus while we do not calculate the distribution of host galaxy properties a priori but rather model individual mergers in order to achieve the resolution necessary to model processes related to star formation and black hole growth, by quantifying our scalings in terms of e.g. $M_{\rm BH}$ and $M_{*,\,\rm tot}$, our methodology is independent of the vast majority of host galaxy properties. These differences manifest in e.g. different final stellar or black hole masses, but do not change any scalings expressed in terms of stellar or black hole mass. It is straightforward to reverse this procedure, for example starting with the QLF and quasar lifetime to determine $\dot{n}(M_{\rm BH})$, converting to $\dot{n}(M_*)$, and using this to predict the MGLF. We can also compare with other quantities, e.g. the SFRF, by convolving $\dot{n}(M_*)$ with the SFR-dependent lifetime $t(\dot{M}_*\,|\,M_*)$.

4.2. *Systematic Uncertainties: Calibrating Merger Timescales/Selection Effects and Gas Fractions*

Before explicitly comparing merger, quasar, and SFR distributions as a function of redshift, we consider systematic uncertainties introduced in the various observed samples by e.g. selection effects and cosmic variance. For quasar populations, these should not be significant sources of uncertainty, as we generally employ hard X-ray samples which are complete to luminosities well below those of interest in our analysis,

especially at the moderate redshifts which we consider in detail (see e.g. Ueda et al. 2003), and have been corrected for obscuring columns with $N_H \lesssim 10^{25}\,\mathrm{cm}^{-2}$. We have also designed our formulation for comparing e.g. quasar and merger populations to be robust with respect to the wide set of parameters varied in our simulations, as discussed in § 3.

However, for a certain "true" merger rate as a function of mass, selection effects will influence the observed merger mass and luminosity functions. Of course, there will be some mass/luminosity completeness limit, but it is straightforward to account for this. More problematic is the fact that different definitions of mergers (i.e. choice of maximum separation in pair-selected samples or strength of tidal features in morphologically identified samples) will, for the same distribution of merger rates, select different sets of "ongoing" mergers. Fortunately, we find in § 3 that merger light curves are quite flat as a function of time, with no strong dependence of observed total luminosity (in the near-UV through near-IR bands we consider) on merger stage. This means that the observed *distribution* of merger luminosities and masses will not be biased by the various sample definitions, only the total number of objects identified as mergers (i.e. vertical normalization of merger luminosity functions). This uncertainty is entirely contained within the parameter $t_{\rm merge}$ defined above; i.e. the total time over which a system would be identified as a merger in an observed sample. In principle, our simulations can be used to determine this quantity from first principles for a given observational sample, convolving predicted galaxy images with the appropriate observational response (including e.g. surface brightness dimming, sky and detector noise) and selection criteria, to calculate the probability along each sightline that the object will be identified observationally.

Such an investigation is beyond the scope of the current paper, but is clearly important for detailed estimates of merger rates as a function of mass and redshift for a uniformly selected merging galaxy sample at different redshifts. Some preliminary results can be obtained by tracking the path of our simulated mergers in Gini-M20 space, a non-parametric morphological classification scheme in which spirals, ellipticals, and mergers occupy distinct regions (Lotz et al. 2004). This quantitative analysis implies that the galaxy interaction may be classified as a merger somewhere between $\sim 0.5-3.0\,$Gyr, depending on the viewing angle, the orbit, the progenitor disk orientations, and the dark matter halo concentration. The median merger time is $\approx 2.0\,$Gyr and it is worth noting that a similar estimate obtains from dynamical time considerations and observations (Patton et al. 2000). In what follows, we simply adopt this as the (constant) $t_{\rm merge}$ for our comparison with observed merger luminosity functions. This is no doubt a rough approximation, but we can test whether variations in $t_{\rm merge}$ will have a significant impact on our conclusions.

Our mapping between e.g. MGLF and QLF is also not *entirely* independent of our simulation parameters, in the sense that a given QLF defines a unique merger mass distribution, but does not constrain the initial (pre-merger) gas fractions of the progenitor galaxies. For a given mass $M_{*,\rm tot}$, the characteristic luminosity at which the merger is observed can be affected by $f_{\rm gas}$, at least for optical/UV samples. Furthermore, we expect that the distribution of gas fractions will be drawn from some PDF, which may depend on galaxy mass. We do not model this (instead adopting a "mean" $f_{\rm gas}$ at a given redshift), primarily because it introduces additional, poorly constrained parameters and because it is unclear to what extent this correlation is driven by more massive systems having undergone previous major mergers (i.e. their pre-merger gas fractions may have been uniform). However, the effect is less important than might be expected, for two reasons.

First, the scaling with mass is not steep (i.e. a factor $\sim 10^2-10^3$ in M_* yields a factor $\sim 2-3$ in $f_{\rm gas}$, similar to the existing uncertainty). Second, our modeling and the observations of Xu et al. (2004); Wolf et al. (2005); Bundy et al. (2005a) imply that the merger mass and luminosity functions do not have steep low mass/faint-end slopes, meaning that it is a good approximation to adopt the typical mean $\langle f_{\rm gas}\rangle$ of galaxies near the MGLF "break". In detail, we have considered our calculations adopting the $f_{\rm gas}$ as a function of late-type galaxy mass from Roberts & Haynes (1994), and find it makes little difference to our predictions (generally modifying them within existing $\sim 1\sigma$ uncertainties). Of course, to the extent that $f_{\rm gas}$ evolves with redshift (see below), this consideration is important in disentangling how much of that evolution owes to a change in the characteristic masses of merging galaxies or to gas depletion through quiescent star formation.

Even if the vertical and horizontal normalizations of the MGLF (equivalently, $t_{\rm merge}$ and $f_{\rm gas}$) were completely undetermined, we show in § 5.1 that the MGLF and QLF *shapes* are not trivially related, and this alone provides a strong test of models of quasar lightcurves and triggering. Moreover, these systematics (contained in $f_{\rm gas}$ and $t_{\rm merge}$) are reasonably well-constrained as described above, and the systematic dependencies in our comparisons are not especially strong over the range in which they are constrained.

We directly infer the sensitivity of our predictions and comparisons between e.g. the QLF and observed MGLF at a given redshift to these systematics. In § 5 we use the formalism described in § 4.1 and our simulations to map the observed QLF to a predicted MGLF, and find that it agrees well with observed MGLFs at $z\sim 0.2$ in the K-band (Xu et al. 2004) and $z\sim 0.7$ at 280 nm (Wolf et al. 2005), for expected values of $t_{\rm merge}\sim 0.5-3\,$Gyr and $f_{\rm gas}\sim 0.1-0.6$. We can quantify this formally: for any given "mean" $t_{\rm merge}$ and $f_{\rm gas}$ at some redshift, the QLF and our methodology define a predicted MGLF, and we can determine the probability (in a χ^2 sense) that the observed MGLF measures this predicted MGLF.

In Figure 6, we plot this for the observed MGLFs at $z\sim 0.2$ and $z\sim 0.7$, where probability contours (essentially measuring the agreement between observed and predicted MGLFs) are shown in $t_{\rm merge}$ and $f_{\rm gas}$. In the K-band ($z\sim 0.2$), this comparison is essentially independent of $f_{\rm gas}$ (as expected from the weak dependence of K-band luminosity on $f_{\rm gas}$ in Equation 1), and depends only weakly on $t_{\rm merge}$ in the range $t_{\rm merge}\sim 1-2\,$Gyr. At 280 nm, the dependence on $f_{\rm gas}$ is stronger, as expected since L_{280} scales with $M_{*,\rm new}\sim f_{\rm gas}M_*$, but our results are still essentially unchanged for reasonable values of typical $z\sim 1$ quasar-producing mergers with gas fractions $f_{\rm gas}\sim 0.2-0.6$ and the broad range of $t_{\rm merge}\sim 0.5-3\,$Gyr. Even considering the effects on both MGLFs simultaneously in the right panel of Figure 6 (which plots the joint probability contours from the K-band and 280 nm MGLFs), our comparison is unaffected over the range $t_{\rm merge}\sim 1-2\,$Gyr and $f_{\rm gas}\sim 0.2-0.6$ (these numbers should not be taken too literally, since the samples derive from different redshifts).

In future samples which determine the merging galaxy luminosity function by uniform, automated selection criteria (see, e.g., Lotz et al. 2006), our comparisons can be made more precise by inferring $t_{\rm merge}$ a priori from the simulations and directly measuring $f_{\rm gas}$ in optical samples. The key point from the above, however, is that our theoretical factor ~ 2

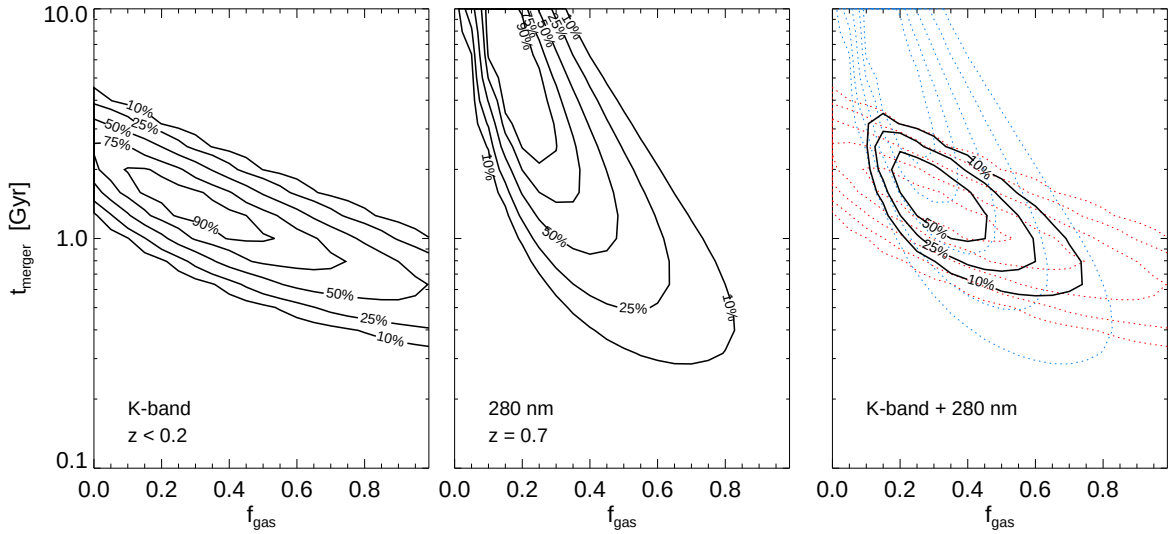

FIG. 6.— Probability contours in host galaxy gas fraction $f_{\rm gas}$ and time the merger is visible in the observed sample $t_{\rm merge}$ for the MGLF in K-band at $z < 0.2$ (left; Xu et al. 2004) and at 280 nm at $z = 0.7$ (middle; Wolf et al. 2005). Contours are shown at 10, 25, 50, 75, 90% as labeled, and quantify the degree to which systematics will change our results. Right panel shows the previous two contour sets (dotted) and the joint (combined) probability contours of both luminosity functions (solid). Allowing these to vary freely yields physically reasonable values, and comparison of the two demonstrates that the dominant systematic uncertainties are different in near-IR and optical/UV MGLFs. Systematics from selection effects and theoretical uncertainties should not change our results over the reasonable ranges of $t_{\rm merge}$ and $f_{\rm gas}$, and will generally be smaller than the effects of cosmic variance.

uncertainty in $t_{\rm merge}$ (which stems from not modeling the full sample selection function and e.g. cosmological orbit distributions) is not important for our conclusions, as any value of $t_{\rm merge}$ in this range still produces a good fit to observed QLFs (i.e. gives a self-consistent mapping between QLF and MGLF). Likewise, variations in merging galaxy gas fraction do not change our results.

Moreover, cosmic variance is likely to overwhelm the systematic normalization issues above for the small volumes probed in observational measurements of merging galaxy statistics. We discuss this further in § 6.2 below, but note that observations with the deep imaging required to identify merging systems have generally been limited to small fields. Somerville et al. (2004b) and Wolf et al. (2005) consider this, and estimate that cosmic variance introduces a systematic factor of $\sim 1.5-2$ in the normalization of the merger luminosity functions. Therefore, it is not warranted to employ a more detailed treatment of merger sample selection effects ($t_{\rm merge}$) or $f_{\rm gas}$ in our modeling, which considers the relation between e.g. the MGLF and QLF, if these are measured in different fields and either (more seriously the MGLF) is significantly affected by cosmic variance, and in any case the introduced systematic uncertainties are comparable to current measurement errors in observed MGLFs.

5. COMPARING THE MERGING GALAXY, QUASAR, AND STAR FORMATION RATE DISTRIBUTIONS

5.1. *The Observed MGLF and QLF*

5.1.1. *The K-Band Merger Luminosity Function*

We examine first the observed K-band pair luminosity function of Xu et al. (2004), at low redshift, $z \lesssim 0.1$. The pair luminosity function is determined from the matched 2MASS-2dFGRS 45,289-galaxy sample of Cole et al. (2001), and agrees well with previous estimates of the local pair fraction (e.g., Zepf & Koo 1989; Burkley et al. 1994; Carlberg et al. 1994; Yee & Ellingson 1995; Patton et al. 1997, 2000) and the B-band luminosity function of paired galaxies (e.g., Xu & Sulentic 1991; Sulentic & Rabaca 1994; Keel & Wu 1995; Soares et al. 1995; Toledo et al. 1999; Conselice et al. 2003), but accounts for effective pair volume corrections instead of treating each member singly with its own $V_{\rm max}$ (since both objects must be identified in a pair to be included in such a sample). Pairs are defined to be within a projected separation $\leq 20\,h^{-1}\,$kpc, with velocity difference (where both redshifts are measured) $< 500\,{\rm km\,s^{-1}}$. Further, the sample is restricted to major mergers, with K-band magnitude differences less than 1 mag (i.e. within a factor ~ 3 in mass), corresponding well to our modeling because these mergers are most likely to trigger starburst and quasar activity and to be visible as peculiar/interacting galaxies for comparison with morphologically selected MGLFs (Mihos & Hernquist 1994a; Walker et al. 1996; Conselice et al. 2003). We consider both their binned data and best-fit Schechter function, with slope $\alpha = -0.30 \pm 0.56$, turnover $M_{K,*} = -23.32 \pm 0.25$, and normalization $\log\phi_* = -3.92 \pm 0.13$ (converted to our cosmology). The distinction between the observed mass function and a constant merger fraction is only marginally significant; moreover, a number of studies measure a cumulative merger fraction. Therefore, we also consider our predictions for a constant merger fraction as a function of mass (given the local stellar mass function from Bell et al. (2003)) with the observed low-redshift value $\sim 2.5 \pm 1\%$ (Xu et al. 2004; Bundy et al. 2005a,b; Bell et al. 2006b).

Figure 7 shows (upper left panel) the predicted QLF from the K-band low redshift MGLF of Xu et al. (2004). Solid circles indicate the observed $z < 0.2$ hard X-ray QLF of Ueda et al. (2003). We rescale the hard X-ray QLF to a bolometric QLF for ease of comparison as in Hopkins, Richards, & Hernquist (2006), using a model of the intrinsic quasar continuum SED following Marconi et al. (2004), based on optical through hard X-ray observations (e.g., Elvis et al. 1994; George et al. 1998; Vanden Berk et al. 2001; Perola et al. 2002; Telfer et al. 2002; Ueda et al. 2003; Vignali et al. 2003), with a hard X-ray reflection component

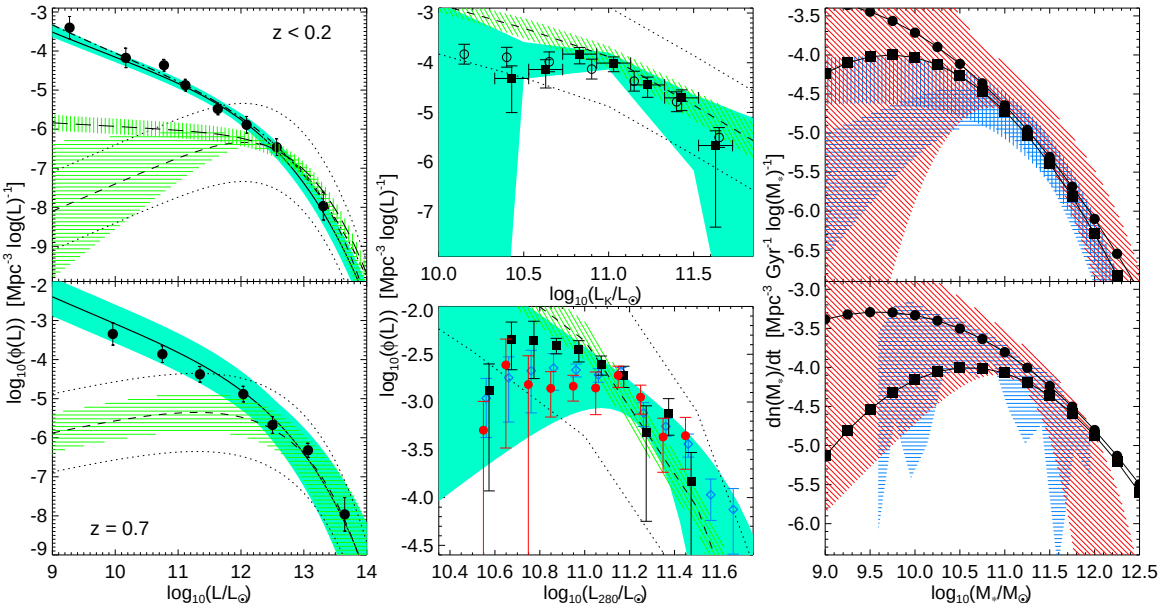

FIG. 7.— *Left*: Predicted QLF from the observed *K*-band $z < 0.2$ (upper; Xu et al. 2004) and 280 nm $z \approx 0.7$ (lower; Wolf et al. 2005) MGLFs, adopting our full model for quasar lifetimes (solid black line; blue shading shows 1σ range based on errors in the observed MGLF), or a "light-bulb" model for the quasar lifetime with t_Q varied to produce the best-fit expected QLF (short dashed; green hatched region shows 1σ range; dotted lines show prediction for t_Q a factor of 10 larger or smaller). Circles show the observed hard X-ray quasar luminosity function of Ueda et al. (2003), rescaled to bolometric luminosity with the corrections from Marconi et al. (2004). The predicted QLF from a constant merger fraction $\sim 2.5 \pm 1\%$ at $z < 0.2$ is also shown (dot-dashed line uses our full model, long-dashed line a "light-bulb" model). *Middle*: Predicted *K*-band $z < 0.2$ and 280 nm $z \approx 0.7$ MGLFs from the QLF of Ueda et al. (2003), lines and colors show the same as the left panels. Observations from Xu et al. (2004) from the 2MASS sample are shown as black squares in the upper panel, and a constant merger fraction ($2.5 \pm 1\%$; given the mass functions of Bell et al. 2003) as circles. In the lower panel, observations from Wolf et al. (2005) are shown as black squares (GOODS), blue diamonds (GEMS), and red circles (GEMS depth on GOODS area). *Right*: Inferred $\dot{n}(M_*)$, the gas-rich merger rate (spheroid birthrate) with a given stellar mass, from the corresponding (*K*-band, upper; 280 nm, lower) observed MGLFs (1σ range, blue horizontal hatched; instead using a constant merger fraction shown as blue vertical hatched), and the corresponding QLF at $z < 0.2$, $z \approx 0.7$, respectively (1σ range, red shaded). Lines with circles and squares show the fitted $\dot{n}(M_*)$ from the QLF used in Hopkins et al. (2006a,b), respectively. In all cases, our modeling demonstrates that the observed QLFs and MGLFs are self-consistent and can be used to predict one another, with all mergers producing bright quasars and all bright quasars initially triggered in mergers. Idealized models of the quasar lightcurve give a very misleading relation between MGLF and QLF, predicting a QLF discrepant by $\gtrsim 6\sigma$.

generated by the PEXRAV model (Magdziarz & Zdziarski 1995). This includes the observed dependence of the optical to X-ray luminosity ratio on luminosity (e.g., Wilkes et al. 1994; Green et al. 1995; Vignali et al. 2003; Risaliti & Elvis 2005; Strateva et al. 2005), but for our purposes adopting the mean observed quasar SED from Richards et al. (2006b) yields a similar result (see e.g. Hopkins et al. 2005d, 2006b for a discussion of the impact of different bolometric corrections on our predictions). For simplicity, we consider only the hard X-ray (2-10 keV) QLF, where attenuation is usually negligible (and note the Ueda et al. (2003) QLF is corrected for columns $N_H < 10^{25}\,\mathrm{cm}^2$).

The black solid line in Figure 7 shows the prediction using the quasar lifetimes fitted from our simulations (described in § 4.1), with the blue shaded region giving the 1σ range allowed based on the errors in the observed MGLF (dot-dashed line is the result adopting instead a constant merger fraction). We show the results for a characteristic $t_{\rm merge} = 2\,$Gyr, corresponding roughly to the time when the galaxies are within $\sim 50\,$kpc of one another in our simulations before merging (appropriate for the maximal projected separation $20\,h^{-1} \approx 30\,$kpc of the observed sample), and $f_{\rm gas} = 0.15$, corresponding to the typical gas fractions of galaxies around the mass of the observed MGLF peak (Roberts & Haynes 1994). However, as shown in § 4.2, our results are relatively insensitive to these choices. Briefly, if we allow $f_{\rm gas}$ and $t_{\rm merge}$ to vary, a formal best-fit is obtained for $f_{\rm gas} = 0.25^{+0.21}_{-0.23}$ and $t_{\rm merge} = 1.7^{+1.2}_{-0.9}\,$Gyr – in other words, the quality of the fit is nearly unchanged for the entire reasonable range of $f_{\rm gas}$ and $t_{\rm merge}$, and these specific values should not be taken too literally. The short dashed line shows the prediction adopting the idealized "light-bulb" quasar model described above (§ 4.1), with again the green horizontal cross-hatched range showing the 1σ range from the observed MGLF (long-dashed line with vertical hatching shows the result for a constant merger fraction). The prediction shown in this case is the best-fit allowing $t_{\rm merge}$, $f_{\rm gas}$, and the quasar lifetime t_Q to vary freely, giving $t_Q \approx 6.3 \times 10^6\,$yr for $t_{\rm merge} = 2\,$Gyr (only the ratio $t_Q/t_{\rm merge}$ is constrained) and $f_{\rm gas} = 0.25$. The dotted lines show the prediction for t_Q larger or smaller by an order of magnitude.

In our model, the faint end of the observed QLF is dominated by quasars with large peak luminosities, but seen in fainter evolutionary states during and after the mergers in which they form. Therefore, the faint end of the predicted QLF is tightly constrained, as it depends on the MGLF near its turnover, where it is most well-determined, and there is little difference between adopting the observed MGLF or a constant merger fraction. With instead a one-to-one correspondence between peak and observed quasar luminosity (dashed lines), the faint-end QLF depends directly on the faint-end MGLF, and is thus poorly constrained. The agreement between the observed QLF and our prediction is good, $\chi^2/\nu \approx 3.41/8 = 0.43$ and it requires no fine-tuning of any parameters. However, even allowing both horizontal and vertical normalizations to vary freely, the *shapes* alone of the quasar and MGLFs rule out a "light bulb" or exponen-

tial lightcurve model at greater than 99.9% confidence, with the best-fit $\chi^2/\nu \approx 29.1/7 = 4.15$ ($\chi^2/\nu \approx 6.45$ adopting a constant merger fraction). Such a fit furthermore requires a quasar lifetime $t_Q \sim 6\times10^6$ yr, at the low extreme of the range indicated by observations (e.g., Martini 2004).

In any model which reproduces the observed $M_{\rm BH}\propto M_*$ relation, $\dot{n}(M_{\rm BH})$ must have approximately the same shape as the merger rate as a function of M_*, itself given approximately by the merger mass function. This shape is observationally well-defined, with a rapid decline above and flattening or decrease below the break luminosity. In Hopkins et al. (2005c), we argue that this is the shape of $\dot{n}(M_{\rm BH})$ (equivalently $\dot{n}(L_{\rm peak})$) implied by the combination of our model for quasar lifetimes with the observed QLF. However, in idealized models of the quasar lightcurve, $\dot{n}(M_{\rm BH})$ must have the same shape as the observed QLF, which cannot be self-consistently resolved with the observed MGLFs. It is true that the faint-end slope of the MGLF is poorly constrained, with $\alpha = 0.30\pm0.56$; however, to be compatible with the faint end slope of the QLF in a light-bulb model (i.e. to steepen the dashed line to match the solid line in Figure 7) requires a 4σ change in α (6σ relative to a constant merger fraction), which seems unlikely, given the large quoted error which includes systematic effects.

Next, we invert this comparison and employ the observed QLF to estimate the MGLF. Figure 7 (upper middle panel) shows this, using the $z<0.2$ hard X-ray Ueda et al. (2003) QLF shown in the upper left panel to determine $\dot{n}(M_{\rm BH})$, and correspondingly $\dot{n}(M_*)$ and $\phi_{\rm gal}(L_K)$, the K-band $z<0.2$ MGLF. Again, the blue range shows the prediction and 1σ range (from errors in the observed QLF) using our full model of quasar lifetimes, with $f_{\rm gas}=0.15$, $t_{\rm merge}=2\,$Gyr. Dashed line and green hatched range shows the same for the "light-bulb" quasar lifetime model, allowing $f_{\rm gas}$, $t_{\rm merge}$, t_Q to be fit as in the upper left panel (producing identical fits), and the dotted lines show the prediction for an order of magnitude larger or smaller t_Q. These can be compared to the black squares, which show the binned MGLF from Xu et al. (2004) (open circles show the constant merger fraction estimate). As expected from the upper left panel, the agreement using our full model of quasar lifetimes is good ($\chi^2/\nu=0.35$), and the agreement with an idealized model of the quasar lifetime is poor ($\chi^2/\nu=3.82$).

The constraints from the observed QLF on the MGLF are significantly weaker than the constraints on the QLF from the observed MGLF. This is not because the QLF is poorly constrained relative to the MGLF (in fact, the opposite is true). Rather, it is because a given interval in observed quasar luminosity has significant contributions from quasars with a wide range of peak luminosities $L_{\rm peak}\gtrsim L$ (and a correspondingly wide range in host galaxy stellar mass), in various stages of evolution. Thus, there are significant degeneracies in predicting the relative contributions from different black hole or host galaxy stellar masses to the observed QLF based only on its observed shape. This is increasingly true at fainter merger luminosities, and therefore we can place only weak constraints on the faint-end $\dot{n}(M_{\rm BH})$ distribution (as discussed in e.g. Lidz et al. 2006). The weak constraints at the high-L_K end, however, owe to larger statistical errors in the QLF. The wide range in the allowed faint-L_K end of the MGLF (demonstrated by the similar predictions given the observed MGLF or a constant merger fraction) is reassuring, in the sense that at low luminosities, selection effects become important in efforts to identify a sample of merging galaxies, but these will not significantly change our result.

As an intermediate stage in these calculations, we have derived the implied $\dot{n}(M_*)$; i.e. the merger rate or birthrate of spheroids with stellar mass, directly related to the black hole "triggering" rate. We show these $\dot{n}(M_*)$ distributions in Figure 7 (upper right panel), where the blue horizontal shaded range shows the 1σ range implied by the observed MGLF of Xu et al. (2004) (vertically shaded range implied by a constant merger fraction), and the red range shows the 1σ range implied by the observed QLF of Ueda et al. (2003) at $z<0.2$. Again, it is clear that the QLF provides poor constraints on the low-mass behavior of $\dot{n}(M_*)$. For comparison, we plot the fitted $\dot{n}(M_*)$ distributions of Hopkins et al. (2006a,b), which were fitted to the combination of optical, soft X-ray, and hard X-ray QLFs (Miyaji et al. 2001; Ueda et al. 2003; Croom et al. 2004; Richards et al. 2005; Hasinger et al. 2005; La Franca et al. 2005). These may rise to lower masses before turning over than is implied by the MGLF, but as we have emphasized above (and shown in e.g. Hopkins et al. 2006b) this produces an essentially identical prediction for the properties of the quasar and remnant red galaxy populations.

5.1.2. *The 280 nm Merger Luminosity Function*

We repeat the analysis in § 5.1.1, for the observed 280 nm UV MGLF of Wolf et al. (2005) from the GEMS and GOODS surveys at $z\approx0.7$. In detail, the galaxies are selected from the overlapping area of COMBO-17 and GEMS, with photometric redshifts $0.65<z<0.75$ and observed $R<24$ (corresponding approximately to a rest-frame U-band). The sample consists of visually identified morphologically selected peculiar/interacting galaxies, and as a consequence there is considerable observational uncertainty in the faint end of the MGLF, where tidal features are especially difficult to detect given surface brightness dimming at higher redshifts. However, as we demonstrate above in the case of the K-band MGLF, our modeling of the QLF is not sensitive to this faint-end behavior.

Figure 7 shows this comparison in the lower panels, in the same manner as the upper panels. The lower left panel shows the predicted QLF using our full model for the quasar lightcurve (solid line), and instead for an idealized "light-bulb" model for the quasar lightcurve (dashed line), with uncertainties as in the upper panels, and dotted lines show the prediction for a fixed quasar lifetime an order of magnitude larger or smaller. We compare to the observed hard X-ray QLF of Ueda et al. (2003), this time at $z=0.7$ (black circles). Whether we use the GEMS or GOODS data makes little difference in the prediction of our model, so we show the result using the GOODS luminosity function, which has a larger number of faint merging galaxies, maximizing the ability of the "light bulb" model to match the data. Again, it is clear that our model provides a good fit, while the "light bulb" model is ruled out at greater than 90% confidence ($\chi^2/\nu=0.159,\ 2.41$ respectively). The shape of the QLF alone provides this qualitative constraint on the quasar lightcurve model, but the vertical and horizontal normalizations also agree well within the reasonable expected ranges $t_{\rm merge}\sim1-3\,$Gyr and $f_{\rm gas}\sim0.2-0.6$. As above, $t_{\rm merge}$, $f_{\rm gas}$, and t_Q are allowed to vary freely in the "light bulb" model, and although the fit is poor, the best-fit values are $f_{\rm gas}=0.3$ and $t_Q=5.8\times10^6$ yr for $t_{\rm merge}=2\,$Gyr. A $\sim4\sigma$ change in the faint-end slope of the MGLF would be required for the "light bulb" model to agree with the QLF, even for the maximal estimate of the number of faint mergers in Wolf et al. (2005).

The lower middle panel of Figure 7 shows the 280 nm MGLF inferred from the $z=0.7$ QLF of Ueda et al. (2003),

in the same style as the upper middle panel. The inferred MGLFs can be compared to those of Wolf et al. (2005) from the GOODS survey, GEMS survey, and a combination of GEMS depth on the GOODS area. The differences in the observed MGLFs at the faint end demonstrate the considerable observational uncertainty here, but the QLF is not sensitive to this faint-end behavior. This is not the case for the idealized "light bulb" model, as demonstrated by the narrow range of the green hatched region even at low luminosities. The constraints are weaker, but the agreement between our model predictions and the observed MGLF is good ($\chi^2/\nu = 0.31$, compared to $\chi^2/\nu = 2.15$ for the light-bulb model).

Finally, we show the $\dot{n}(M_*)$ distribution implied by the MGLF of Wolf et al. (2005) (lower right panel) as the blue shaded range, The range implied by the QLF at $z = 0.7$ is indicated as the red shaded range, with the fits to $\dot{n}(M_*)$ used in Hopkins et al. (2006a,b). The implied $\dot{n}(M_*)$ distributions at $z = 0.7$ and $z < 0.2$ from 280 nm and K-band observations, respectively, can be compared to infer the evolution of merger rates and quasar birthrates as a function of mass, but we caution against taking this comparison too far. The samples use various selection criteria, are from different surveys, are not in the same wavebands, and have different dependence on gas fraction. Therefore, the potential systematic effects may be quite different between the two.

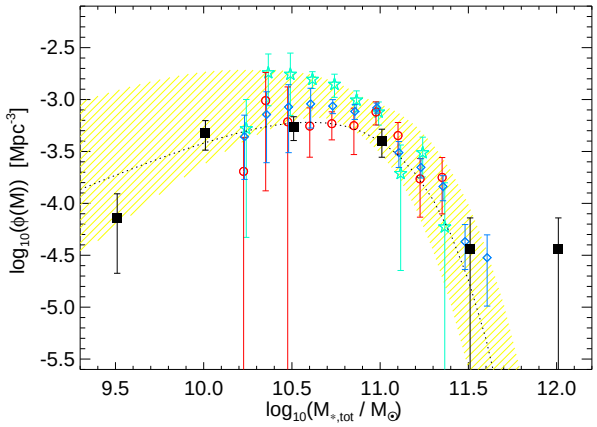

FIG. 8.— Merger mass function at $z \approx 0.7$, predicted from our modeling with the observed 280 nm MGLF of Wolf et al. (2005) (colored), and directly calculated from near-IR and optical observations in Bundy et al. (2005a) (black). Points converted from the 280 nm observations in Figure 7 are shown as cyan stars (GOODS), blue diamonds (GEMS), and red circles (GEMS depth on GOODS area), and the $\sim 1\sigma$ allowed mass function from our modeling as the yellow shaded region. Black squares show the binned mass function from Bundy et al. (2005a), black dotted line shows the best-fit Schechter function. The agreement implies that our simulations reliably map between MGLFs and merger stellar or black hole mass functions.

5.1.3. *Merger Mass Functions*

We repeat our analysis using the morphologically separated mass functions of Bundy et al. (2005a,b) from GOODS and DEEP2. Stellar masses are determined by fitting to optical spectroscopy and near-IR photometry, and we adopt the mass functions for objects visually classified as mergers (following Brinchmann et al. 1998) with ACS morphologies. This gives a binned merger stellar mass function determined in each of the intervals $z = 0.2-0.55$, $z = 0.55-0.8$, and $z = 0.8-1.4$, spanning $M_* \sim 10^9 - 10^{12}\,M_\odot$ (see Figure 8 below for a detailed comparison with the $z = 0.55-0.8$ mass function). In each case, the observed merger mass function implies a QLF in good agreement with the observations of Ueda et al. (2003) ($\chi^2/\nu \approx 0.85,\ 0.52,\ 0.98$ for $z = 0.2-0.55,\ 0.55-0.8,\ 0.8-1.4$, respectively), and the implied mass function from the QLF, albeit less well-constrained, is consistent with the observed mass functions. These observations also consistently rule out a "light bulb" or similarly idealized model for the quasar lightcurve at $\gtrsim 10\sigma$.

5.2. *Comparison of Merger Mass and Luminosity Functions*

While the agreement between quasar and merger statistics is encouraging, we now test our modeling of the MGLF directly by comparing the observed 280 nm MGLF of Wolf et al. (2005) to the measured merger mass functions of Bundy et al. (2005a,b). We consider the Bundy et al. (2005a) mass functions determined from the GOODS field, with redshifts $0.55 < z < 0.8$, similar to the $0.65 < z < 0.75$ range considered in Wolf et al. (2005). In both cases, optical or near-IR morphologies are used to visually select merging systems, so the ambiguity in selection effects is minimized.

Figure 8 shows the inferred merger mass function using our simulated $P(L_{280}\,|\,M_*)$ to convert $\phi(L_{280})$ directly to $\phi(M_*)$. The observations of Wolf et al. (2005), converted to a mass function, are shown by the symbols indicated in the caption. Alternatively, adopting the $\sim 1\sigma$ range in allowed fitted MGLFs from Wolf et al. (2005) and converting this to a merger mass function yields the shaded yellow range. The range shown can also be thought of as a range in gas fraction, with $f_{\rm gas} \approx 0.15-0.30$. The observed merger mass function of Bundy et al. (2005a) is shown as the black squares, with the black dotted line showing the best-fit Schechter function.

The merger mass function implied by the MGLF and our modeling agrees well with that observed, suggesting that we are capturing the critical dependence of observed merger luminosities on host properties. Coupled with observations of a similar relation between black hole and spheroid mass at these redshifts (e.g., Peng et al. 2006), this observationally supports multiple implicit levels of our modeling.

5.3. *The Distribution of Star Formation Rates*

Having determined $\dot{n}(M_*)$ from the QLF or MGLF, we can convolve instead with the time each merger spends in some interval in SFR, $\dot{M}_*$ (Equation [5]), to determine the observed SFRF in mergers. Figure 9 shows the results given $\dot{n}(M_*)$ (specifically $\dot{n}(M_{*,\rm new})$) determined from the 280 nm observed peculiar/interacting luminosity function of Wolf et al. (2005) at $z = 0.7$ from GEMS and GOODS (solid line with 1σ blue shaded range). We compare this to the observed SFRF of the same merging galaxy sample, determined in Bell et al. (2005). Note that while Bell et al. (2005) determine the SFRF and relative number density as a function of morphology, they do not determine the absolute SFRF normalization (i.e. proper effective volume correction), and so we adopt that inferred by Le Floc'h et al. (2005) at $z = 0.6-0.8$ from Spitzer in the Chandra Deep Field South. Red points are observations with no correction for incompleteness below $\dot{M}_* \sim 10\,M_\odot{\rm yr}^{-1}$, while black points have been corrected for incompleteness at low SFR based on the comparison of GEMS and GOODS luminosity functions from Wolf et al. (2005).

The agreement is good, implying that we are properly modeling the relation between the optical/UV luminosity of mergers and at least the statistics of the induced star formation as a function of time. This is not trivial, as there is no one-to-

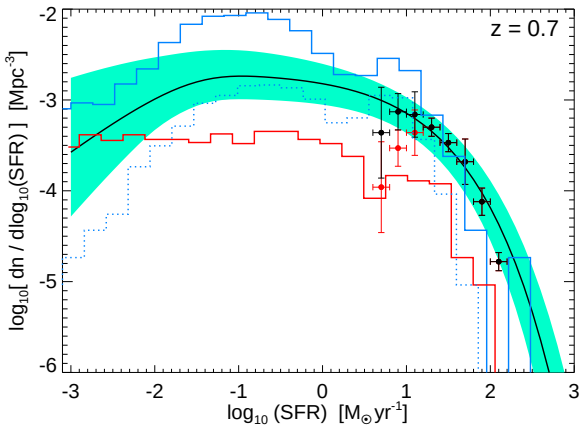

FIG. 9.— Distribution of star formation rates in mergers at $z = 0.7$, inferred from our modeling and the $z = 0.7$, 280 nm MGLF of Wolf et al. (2005) (solid line). Shaded range shows 1σ range based on observational errors in the MGLF. Circles show the observed SFRF of Bell et al. (2005) at the same redshift (black, corrected for completeness; red, uncorrected), normalized with the observed IR luminosity functions of Le Floc'h et al. (2005). Red line shows the predicted SFRF owing to major mergers from the semi-analytic models of Somerville et al. (2001), blue lines include minor mergers. Solid lines adopt $t_{\rm merge} \sim 10\,t_{\rm dyn} \sim$Gyr, dotted lines $t_{\rm dyn} \sim 10^8$ yr as the maximum time since the last merger. The agreement implies that our modeling reliably predicts the merger-driven SFR distribution from a given MGLF or QLF. Note the increasing importance of minor mergers at low SFR.

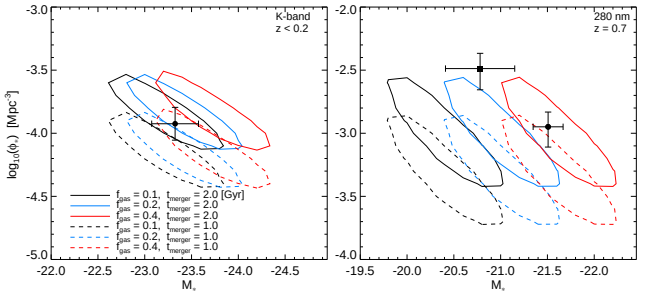

FIG. 10.— Contours of the 1σ allowed Schechter function parameters M_*, ϕ_* (assuming $\alpha = -0.5$) for the MGLF in K-band at $z < 0.2$ (left) and at 280 nm at $z = 0.7$ (right), assuming different values for the gas fraction $f_{\rm gas}$ and selection efficiency (time during which the merger will be identified as such) $t_{\rm merge}$, as labeled. Points with error bars show the measurements at the corresponding frequency and redshift of Xu et al. (2004) from the 2MASS-2dFGRS survey in K-band and Wolf et al. (2005) from GOODS (square) and GEMS (circle) at 280 nm (observations rescaled assuming $\alpha = -0.5$). The QLF can significantly constrain the allowed MGLF parameters ϕ_* and M_*, modulo systematic uncertainty in the merger timescale $t_{\rm merge}$ (i.e. sample selection effects) and typical merging galaxy gas fraction $f_{\rm gas}$.

one correspondence between the 280 nm luminosity and SFR (as optical/UV lightcurves are flat while SFRs change by orders of magnitude). Also note that, because both the 280 nm magnitude and SFR distributions are functions of $M_{*,\rm new}$ (as opposed to $M_{*,\rm tot}$), the relation between the two is independent of $M_{*,\rm tot}$ and $f_{\rm gas}$.

It is also of interest to compare our prediction for the distribution of mergers and SFRFs to that from semi-analytic models. In general, this is difficult, as the events of interest are not mergers of dark matter halos, but involve the luminous galaxies themselves, in which the galaxies are of comparable mass and have a large supply of cold (rotationally supported) gas. Furthermore, the exact requirements for triggering starbursts and AGN depend on, for example, the pressurization of ISM gas, star formation recipes, and the distribution of orbital parameters in the mergers (e.g., Hernquist & Mihos 1995). We have specifically chosen to quantify the properties of mergers in terms of e.g. $L_{\rm peak}$, $M_{*,\rm tot}$, and $M_{*,\rm new}$, in a manner which suppresses these dependencies, in order to relate merger, starburst, and quasar populations independent of these detailed (and difficult to model) cosmological distributions. It is therefore outside the scope of this paper to consider a detailed comparison of merger rates as a function of these conditions as implied by e.g. our semi-empirical modeling, semi-analytic models, and cosmological simulations. However, we briefly consider a comparison between our predicted merger-driven SFRF and that predicted by semi-analytic models in Figure 9.

We show as the red solid line the SFRF predicted owing to major mergers (mass ratios less than ∼3:1), and as the blue solid line the SFRF owing to "minor" mergers (mass ratios less than ∼10:1), calculated at $z = 0.7$ from the semi-analytic models of Somerville et al. (2001, 2004a). We consider a galaxy to be "merging" if it has undergone a merger within a time $\sim 10\,t_{\rm dyn} \sim$Gyr (blue dotted line shows the minor-merger prediction for a merger time $\sim t_{\rm dyn} \sim 10^8$ yr). There is broad agreement, suggesting that the rate of gas-rich mergers in the standard CDM cosmology is appropriate to that implied by our modeling and the observations. However, it is only with the inclusion of some "minor" mergers that the semi-analytic model predictions match the observations and our predictions from the QLF and MGLF, suggesting that our implied merger rates as a function of final, total stellar mass may have contributions from a wide range of mass ratios ∼10:1 to 1:1 (which we implicitly account for by expressing the merger rate in terms of the final mass and peak quasar luminosity), increasingly dominated by major mergers at the high-mass end. This comparison, though, is sensitive to the estimate of the observable timescales in the semi-analytic model (but see e.g., Bell et al. 2006b, for comparison with these merger rate estimates).

6. THE EVOLUTION OF MERGER LUMINOSITY FUNCTIONS AND STAR FORMATION RATE DISTRIBUTIONS

6.1. *Merger Luminosity Functions*

Now, we use the observed QLF to predict the MGLF at redshifts where measurements do not yet exist. We have seen that the observed QLF is insensitive to the number of low-mass mergers. If we assume that the MGLF is well-fitted by a Schechter function,

$$\phi(M) = \phi_*\, 10^{0.4\,(M-M_*)\,(\alpha+1)} \exp\left\{-10^{0.4\,(M-M_*)}\right\}, \qquad (11)$$

this means that the QLF has almost no power to constrain α. However, if we assume a specific α, we can then fit the observed QLF to determine the allowed range of ϕ_* and M_*.

Figure 10 shows this determination of ϕ_* and M_*, assuming a constant $\alpha = -0.5$, for both the K-band $z < 0.2$ and 280 nm $z = 0.7$ MGLFs, compared to the observations of Xu et al. (2004) and Wolf et al. (2005). The observed MGLF ϕ_* and M_* have been re-fit assuming the same $\alpha = -0.5$. For each wavelength, we show the contours enclosing the 1σ range of ϕ_*, M_* for a given gas fraction and $t_{\rm merge}$. As expected from § 4.2, the theoretical uncertainty in $t_{\rm merge}$, $f_{\rm gas}$ is generally unimportant relative to the observational factor ~ 2 uncertainties. In principle, the number of observed mergers scales with the selection efficiency $t_{\rm merge}$ and their luminosities with $f_{\rm gas}$, such that they independently control the prediction of ϕ_* and M_*, respectively. If there were no errors in observations of the

relevant luminosity functions, comparison of M_* alone could fix the distribution of $f_{\rm gas}$. However, even small errors in the observed luminosity functions make ϕ_* and M_* strongly degenerate parameters, and the choice of α introduces another, albeit well-known, degeneracy.

Given these degeneracies, we focus on the more robust prediction of the luminosity density. The full luminosity density, $\rho_L = \phi_* L_* \Gamma(\alpha+2)$, technically includes the order unity correction from the integrated faint-end contribution, $\Gamma(\alpha+2)$, which our modeling has little power to constrain from the observed QLF. However, the quantity $\phi_* L_*$ is well-determined, and in Figure 11 we show our predictions for this combination (i.e. neglecting the $\Gamma(\alpha+2)$ correction, or equivalently assuming $\alpha=-1$ or $\alpha=0$, although the corrections from α are small for the reasonable range $-1.5 \leq \alpha \leq 0.5$). Most observational estimates of ρ_L have been in the *B*-band, so we show the predicted luminosity density in *K*-band (left) and *B*-band (right), as a function of redshift from $z=0-6$, based on the combined Miyaji et al. (2001); Ueda et al. (2003); Croom et al. (2004); Richards et al. (2005); Hasinger et al. (2005); La Franca et al. (2005) QLFs. The *B*-band (440 nm) calculation of host galaxy luminosities is identical to our calculation at 280 nm (see also Hopkins et al. 2006b, for a full calculation); the luminosities and scaling with $M_{*,\rm new}$ are nearly identical (see Table 1) modulo a nearly mass-independent $M_B - M_{280} \sim 0.9$ (reflecting the mean young stellar population age $\sim 0.5\,$Gyr). We compare with the $z<0.2$ MGLF measurement of Xu et al. (2004), the merger IR and *B*-band luminosity densities of Conselice et al. (2003, 2005) at mean redshifts $z=0.88,\ 1.68,\ 2.22,\ 2.71$, the peculiar/interacting galaxy mass functions of Bundy et al. (2005a,b) at $z=0.2-0.55$, $z=0.55-0.8$, and $z=0.8-1.4$, the $z<0.1$ optical pair luminosity function of Toledo et al. (1999), and *B*-band peculiar luminosity densities from Brinchmann et al. (1998) at $z=0.2-0.5$, $z=0.5-0.75$, and $z=0.75-1.0$.

In order to predict ρ_L at each redshift from the QLF, we must adopt a typical gas fraction $f_{\rm gas}(z)$. In Figure 11 the dotted line is for a constant $f_{\rm gas}=0.3$, where this value is chosen because it provides a best fit to the cumulative observations plotted (considering the fit to the full MGLF where possible). The solid line assumes an exponentially declining gas fraction with cosmic time, $f_{\rm gas} = 10^{-t/t_{\rm H}}$ where $t_{\rm H}$ is the Hubble time, such that $f_{\rm gas}=1$ at early times and $f_{\rm gas}=0.1$, similar to the Milky Way, at present. This gives an *e*-folding time for $f_{\rm gas}$ of $t_{\rm H}/\ln(10) \approx 6\,$Gyr, similar to that expected for quiescent spirals following a Schmidt-type star formation law (Kennicutt 1998; Rownd & Young 1999; Martin & Kennicutt 2001; Springel & Hernquist 2003a; Li et al. 2005, 2006). Comparing with the evolution of the distribution of cold (rotationally supported) gas mass fractions in galaxy mergers (with total baryonic mass above $10^{10}\,M_\odot$) in the semi-analytic models of Somerville et al. (2004a), we find that these cosmological models predict a similar evolution in the mean gas fraction. The yellow shaded range shows the 1σ allowed range inferred from the QLF, for the evolving $f_{\rm gas}$ case (uncertainties are similar for constant $f_{\rm gas}$).

Although it is clear that the observations do not strongly distinguish between the two cases, and we caution that we have assumed a constant selection efficiency $t_{\rm merge}$ despite different observed sample selection criteria and different redshifts, there is a significantly better fit to the combination of luminosity density and MGLF observations in the case of the exponentially declining gas fraction ($\chi^2/\nu = 0.4$ compared to $\chi^2/\nu = 2.1$). This distinction is derived from the *B*-band and 280 nm data; the *K*-band is relatively insensitive to $f_{\rm gas}$ and does not significantly constrain this evolution. That the exponential decline in gas fraction is preferred by the data is expected, and the observations are not accurate enough to significantly constrain the timescale or detailed functional form of the decrease in gas fraction with time, but this demonstrates the key qualitative behavior, that merging galaxies were more gas rich in the past and that these measurements can constrain that evolution through the evolution in $M_*(z)$.

It is clear from the figure that our predictions for the luminosity density are narrowly constrained, generally within a factor ~ 2 at all redshifts, with the errors dominated by uncertainties in the observed QLF (and thus potentially improved by future, high redshift complete samples which can constrain the QLF break luminosity at a range of redshifts) as opposed to fitting degeneracies. The variation owing to different gas fractions is small in the *K*-band, as expected, but enters approximately linearly into the *B*-band luminosity densities. Improved constraints on the *K*-band MGLF measurements and extension of *B*-band MGLF measurements to higher redshifts can provide a strong test of whether the consistent relation between merger and quasar populations this modeling demonstrates at $z \lesssim 3$ remains true at high redshifts.

6.2. *The Merger-Driven Star Formation Rate Distribution*

Following § 5.3 but beginning from the observed QLF instead of the MGLF, we can predict the SFRF as a function of redshift. Figure 12 shows the results of this calculation at several redshifts $z=0-3$ (as labeled), from the fit to the combined Miyaji et al. (2001); Ueda et al. (2003); Croom et al. (2004); Richards et al. (2005); Hasinger et al. (2005); La Franca et al. (2005) QLFs. The dashed line shows the prediction from the MGLF (as opposed to the QLF) at $z=0.7$ from Figure 9. Points at $z=0.7$ show the observations (Bell et al. 2005; Le Floc'h et al. 2005) as in Figure 9. We adopt our rough estimate $f_{\rm gas} = 10^{-t/t_H} \approx \exp(-t/6\,{\rm Gyr})$. The evolution in the SFRF is predominantly a reflection of the luminosity evolution of the QLF, as the break in the QLF evolves towards larger luminosities with redshift, implying that typical corresponding black hole and host galaxy masses must evolve similarly. Our assumption that the typical gas fractions rise with redshift also increases the SFR for a given total (final) mass, resulting in a further factor ~ 3 increase in $M_{*,\rm new}$ from $z=0.2-2$. Comparing e.g. the specific star formation rate distributions as a function of stellar mass, age, and redshift from our simulations and observed in Bauer et al. (2005); Feulner et al. (2005); Pérez-González et al. (2005); Papovich et al. (2006) yields a similar self-consistent "downsizing."

Although this calculation suggests a form for e.g. the ULIRG and LIRG IR luminosity functions, we caution that we do not model re-radiation of absorbed light by dust and are not yet in a position to predict these properties. However, a rough calculation shows that we expect ULIRGs counts to be consistent with our modeling (Hopkins et al. 2006b). We defer a more thorough calculation of the IR spectrum, including dust heating, re-radiation and line emission, to future work.

We can integrate the SFRF calculated at each redshift to determined the SFR density in mergers as a function of redshift, as shown in Figure 13. The solid black line is our prediction assuming $f_{\rm gas} = 10^{-t/t_H}$ as estimated in § 6.1, with shaded 1σ range based on the errors in the observed QLF and degeneracies in fitting. We also show the predictions for a constant

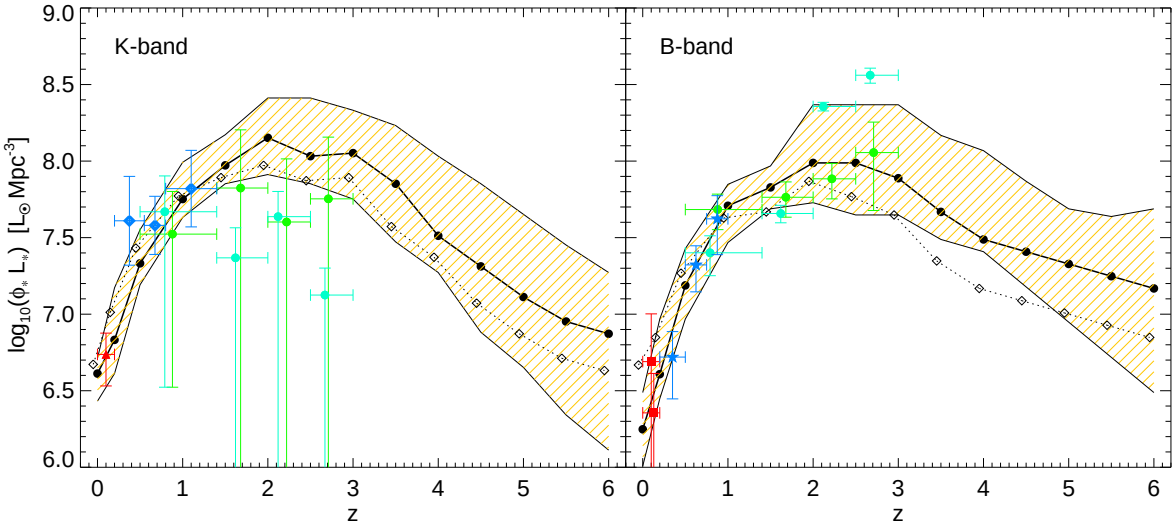

FIG. 11.— Predicted luminosity density contributed by merging galaxies in *K*-band (left) and *B*-band (right), as a function of redshift. Solid line assumes a gas fraction $f_{\rm gas} = 10^{-t/t_H}$, dotted line assumes a constant $f_{\rm gas} = 0.3$ at all z. Yellow shaded range shows the 1σ allowed range inferred from the QLF, for the evolving $f_{\rm gas}$ case (errors are similar for constant $f_{\rm gas}$). Observations are shown from Xu et al. (2004) (red triangle), Bundy et al. (2005a,b) (blue diamonds), Conselice et al. (2003, 2005) (circles; HDF-N in cyan, HDF-S in green), Toledo et al. (1999) (red squares), and Brinchmann et al. (1998) (blue stars). The observed mass/luminosity density in mergers and its evolution is consistent with that required if all bright quasars are triggered in mergers *and* the converse, that all mergers trigger bright quasars. The quasar luminosity function and our modeling can be used to predict the merger mass and luminosity density at all redshifts where the QLF break is reasonably constrained.

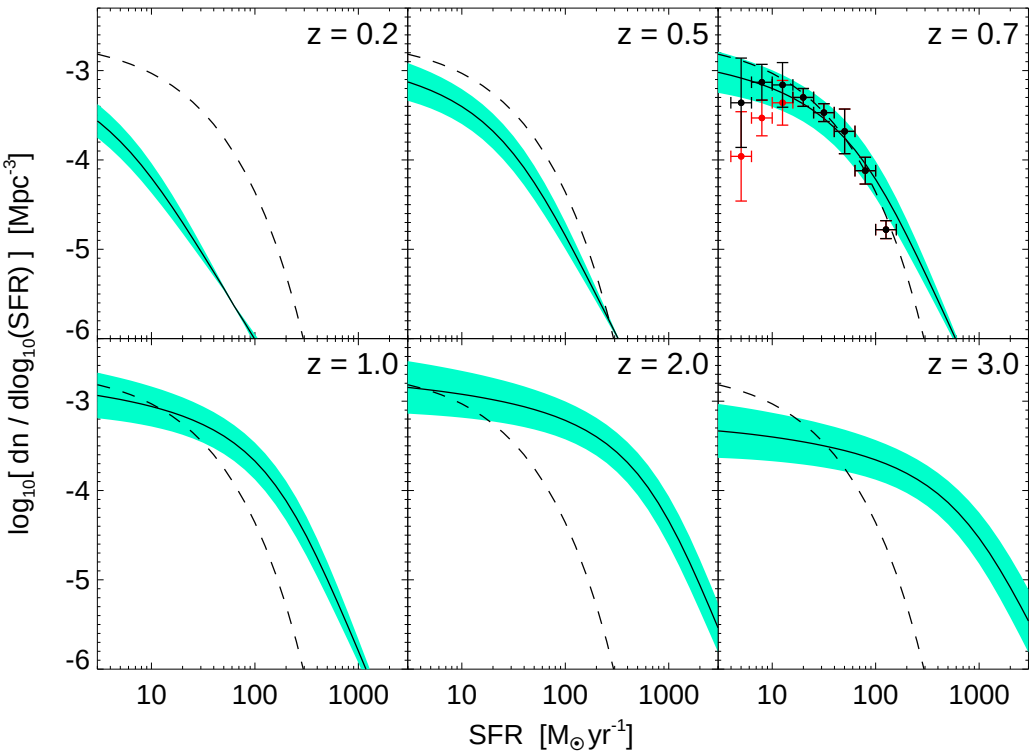

FIG. 12.— Inferred SFRF in mergers from the QLF as a function of redshift (black lines) at the redshifts shown. The shaded area shows the 1σ range from errors in the observed QLF and uncertainties in fitting to it. Observations of Bell et al. (2005); Le Floc'h et al. (2005) are shown at $z = 0.7$ in the manner of Figure 9, and the dashed line in each panel shows the prediction from the 280 nm MGLF of Wolf et al. (2005) from Figure 9 at $z = 0.7$ for comparison. The dashed line and solid line at $z = 0.7$ are slightly different because the former is predicted from the observed merger luminosity function at that redshift, the latter from the observed QLF. The QLF alone allows us to reasonably constrain the distribution of star formation rates in mergers, over a wide range of redshifts where observations are not available.

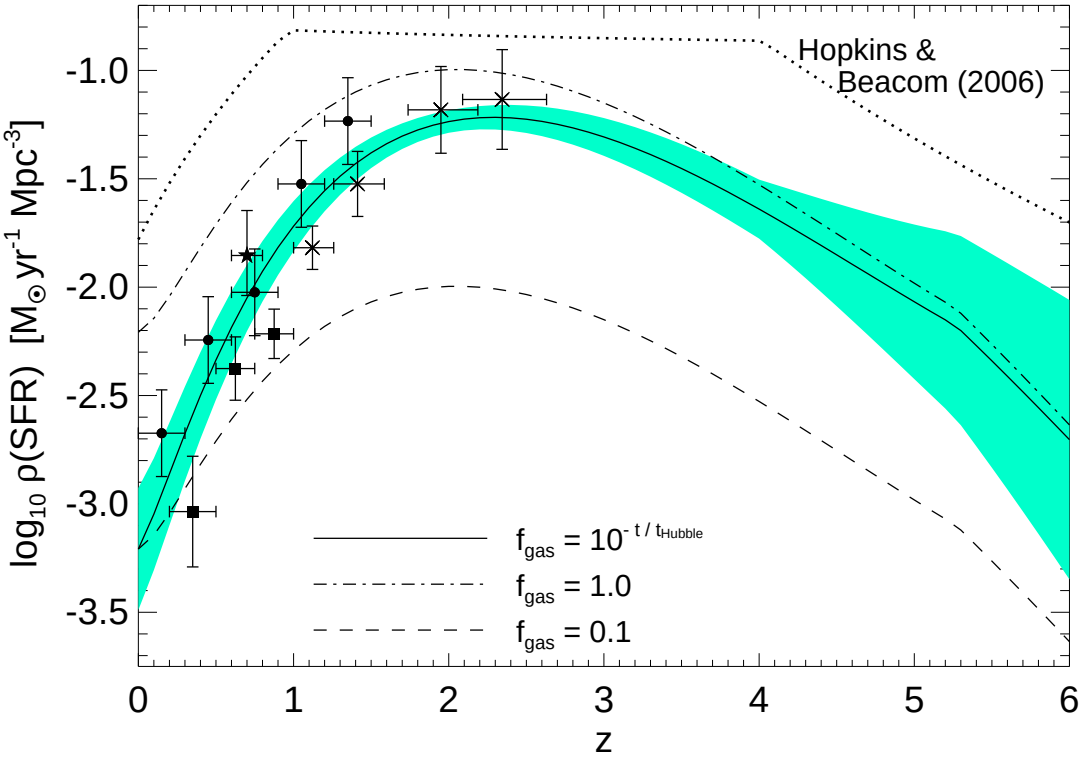

FIG. 13.— Star formation rate density in mergers, inferred from the quasar luminosity function assuming an average gas fraction $f_{\rm gas} = 10^{-t/t_H} = \exp(-t/6\,{\rm Gyr})$ (solid line). The shaded area shows the 1σ range allowed (owing to degeneracies in fitting to the observed QLF). Note that adopting the steeper faint-end slope estimates from the deeper GOODS subsample of Wolf et al. (2005) systematically increases our prediction by a factor $\sim 50\%$ (at the upper range of the 1σ uncertainty). The dot-dashed line and dashed lines show the result assuming a constant gas fraction $f_{\rm gas} = 1.0$ and $f_{\rm gas} = 0.1$, respectively (for clarity, errors are not shown, but they have identical form). Dotted lines show the estimated total (extinction-corrected) star formation rate density from Hopkins & Beacom (2006). Observations of the SFR density in mergers at various redshifts are shown from Bell et al. (2005) (star), Brinchmann et al. (1998) (squares), Pérez-González et al. (2005) ($\times$'s; from the estimate of the ULIRG contribution to the SFR density), and Menanteau et al. (2001, 2006) (filled circles). The $f_{\rm gas} = 1$ line can also be thought of as the total rate at which stellar mass is "moved" or "generated" onto the red sequence by quasar-producing gas-rich mergers. The QLF alone can be used as an independent constraint on the merger-driven SFR density of the Universe; the SFR density in mergers must rise from $\sim 1\%$ of the total SFR density at $z = 0$ to $\sim 15-25\%$ at $z = 1$ and $\sim 30-50\%$ at $z = 2$.

$f_{\rm gas}$ = 1.0 (dot-dashed) or $f_{\rm gas}$ = 0.1 (dashed) (errors similar to the case shown). The solid line effectively interpolates between a high-gas fraction era at $z \gtrsim 2$ to present characteristic low gas fractions $f_{\rm gas} \sim 0.1$ at $z = 0$. The predicted evolution in ρ(SFR) is understood from the QLF. The time-averaged growth rate of black holes is $j_L/\epsilon_r c^2$, where j_L is the quasar luminosity density, so if all bright quasars (i.e. most of j_L at moderate/high redshift) come from spheroid-forming mergers with $M_{*,\rm new} \approx f_{\rm gas} M_* \approx f_{\rm gas} M_{\rm BH}/\mu$ ($\mu \approx 0.001$) we expect $\rho({\rm SFR}) \sim f_{\rm gas}\, j_L/\mu\, \epsilon_r\, c^2$.

For comparison, we show the total (integrated over all morphological types), extinction-corrected SFR density estimated in Hopkins & Beacom (2006) (similar to e.g. Cole et al. 2001, Hopkins 2004 or predictions of cosmological simulations, e.g. Springel & Hernquist 2003b, Hernquist & Springel 2003) as the dotted line. Observations of the SFR density in merging/peculiar systems are plotted, from Bell et al. (2005), Brinchmann et al. (1998), and Menanteau et al. (2001, 2006). The estimate of the SFR density in ULIRGs from Pérez-González et al. (2005) is also shown, but we caution that while these objects are associated with mergers at low redshift, dusty, more concentrated disks at high redshift may contribute to this population.

The agreement between the observations of the SFR density in merging galaxies as a function of redshift and our modeling is good, implying that the QLF can be used as an independent, albeit indirect constraint on the star formation history in mergers and the contribution of merger-driven starbursts to present stellar populations. Systematic uncertainties in the observations are still a concern; e.g. the observations of Brinchmann et al. (1998) may be incomplete owing to dust extinction; see Menanteau et al. (2006). More important, cosmic variance in likely to overwhelm the systematic normalization issues above for the small volumes probed in the observations shown. The difficulty of identifying mergers without deep imaging has naturally limited the effective volume of most such measurements. Somerville et al. (2004b) and Wolf et al. (2005) discuss this for several of the fields we have considered (e.g., GOODS, GEMS, HDF), and for the specific application to different morphological classifications, and they estimate a factor of $\sim 1.5-2$ uncertainty in their estimates from GOODS. Lacking a sufficiently large volume to overcome cosmic variance, we should ideally compare measurements from the same fields. That is, regardless of cosmic variance in a particular field, the observed QLF, MGLF, and merging galaxy SFRFs in that field should be consistent. In fact, if we limit our comparisons in this manner, we find very good agreement between the observations and our predictions (see e.g. § 5). The problem here is that again, existing fields with deep space-based imaging are too small to contain rare, luminous quasars. In general, our predictions from the QLF may be more representative of the cosmic mean, as they agree with the observed QLFs from large volume surveys such as the SDSS (e.g., Richards et al. 2005, 2006a).

Despite systematic uncertainties, the trend in ρ(SFR) appears robust, and we can make several comparisons between the SFR density in mergers and the total SFR density estimated by Hopkins & Beacom (2006). Uncertainties in this comparison are dominated by the factor $\sim 2-3$ scatter in observational estimates of the total SFR density, rather than uncertainties in our predictions. Regardless, we confirm the results of various observational estimates of merger fractions and their evolution with redshift (Le Fèvre et al. 2000; Patton et al. 2002; Conselice et al. 2003; Lin et al. 2004; Bundy et al. 2004; Conselice et al. 2005; Bell et al. 2005; Wolf et al. 2005), namely that at $z \lesssim 1$, star formation triggered in mergers contributes only a small fraction to the SFR density of the Universe, but this increases near the era of peak merger and quasar activity at $z \gtrsim 2$. Specifically, from Figure 13 we predict that only $\sim 1\%$ of the SFR density at $z = 0$ is driven by mergers, and even assuming a maximal $f_{\rm gas} = 1.0$ in all mergers increases this only to $\sim 10-20\%$ (setting a strong upper limit). The predicted contribution from mergers rises to $\sim 15-25\%$ by $z = 1$, with an upper limit $\sim 35\%$ ($f_{\rm gas} = 1$). At $z = 2$, the contribution from mergers increases to $40^{+8}_{-6}\%$ of the cumulative SFR density, and $35^{+10}_{-8}\%$ at $z = 3$. Above these redshifts, the best-fit prediction approximately preserves these ratios, but the uncertainties become large. Thus, spiral galaxies (and increasingly irregular galaxies at higher redshift, e.g. Cross et al. (2004); Daddi et al. (2004); Somerville et al. (2004a)) dominate the SFR density at $z \lesssim 2$, even assuming the most optimistic $f_{\rm gas} = 1.0$ pure gaseous mergers, with the contribution from mergers rising to a comparable but not dominant $\sim 30-40\%$ at higher redshifts.

These predictions do depend systematically on the faint-end slope of the MGLF, or equivalently the low-mass slope of the merger mass function. We have adopted typical measured values from Xu et al. (2004); Bundy et al. (2005a,b), but if the low-mass incompleteness is large and we instead adopt the maximally steep slope from Wolf et al. (2005), this increases our predictions by $\sim 50\%$, enhancing the merger-driven contribution to ρ(SFR) to $\sim 30\%$ at $z = 1$ and $\sim 60\%$ at $z = 2$. Moreover, $f_{\rm gas}$ is somewhat uncertain, but it enters approximately linearly in Figure 13, so our prediction can be rescaled with improved observational constraints on $f_{\rm gas}$.

By convolving our predicted rate of spheroid formation as a function of redshift with the characteristic gas fraction as a function of redshift, we can estimate a "mean" $f_{\rm gas}$ for spheroid-producing mergers leading to spheroids of a given $z = 0$ mass. The redshift-dependent rate of spheroid formation is given in Hopkins et al. (2006b), but is essentially determined by the merger rates as a function of total, final mass at each redshift. For example, the $f_{\rm gas} = 1$ line in Figure 13 can also be thought of as the total rate at which stellar mass is "moved" from the blue sequence to the red sequence by quasar-producing, gas-rich mergers. Because the implied merger activity peaks at $z \gtrsim 2$ corresponding to the peak of quasar activity, assuming $f_{\rm gas} = 10^{-t/t_H}$ gives a nearly constant characteristic mean gas fraction $\sim 60\%$ for essentially all spheroid masses of interest ($M_* \gtrsim 10^8 M_\odot$). The old ages of spheroids coupled with the expected increase in disk gas fractions at high redshift means that it is indeed a good approximation to assume that most spheroids are formed in quite gas-rich mergers. This is supported by observations, as e.g. Hoekstra et al. (2005) find from stellar population analysis that elliptical galaxies must have formed much of their stellar mass around the time of the elliptical-producing event. This does not, of course, prohibit subsequent spheroid-spheroid mergers, which will not trigger star formation or quasar activity.

7. QUASAR HOST GALAXY LUMINOSITY FUNCTIONS

Given the luminosity function of merging galaxies which produce quasars, it is relatively simple to convert this into the expected luminosity function of quasar "host galaxies" (HGLF), but we must first define what we mean by quasar "hosts." If we include e.g. starbursts with buried,

low-luminosity X-ray AGN then we will recover a similar merger luminosity function to that we calculate from the X-ray QLF. However, most efforts to measure the distribution of AGN host galaxy luminosities (e.g., Bahcall et al. 1997; McLure et al. 1999; Falomo et al. 2001; Hamilton et al. 2002; Jahnke & Wisotzki 2003; Dunlop et al. 2003; Floyd et al. 2004; Vanden Berk et al. 2006) have considered hosts of bright, *optical*, broad-line quasars. In our modeling, this phase of quasar activity is associated with the "blowout," i.e. the final stages of black hole growth, when the surrounding gas is expelled and heated and the black hole is briefly rendered a bright optical source before accretion shuts down. We consider this in detail in Hopkins et al. (2006b) (Equation [26]) and derive the useful mean relation from our simulations

$$\frac{L^{\rm qso}_{\rm B,\,obs}}{L^{\rm gal}_{\rm B,\,obs}} = 7.9\,\frac{1}{f_{\rm gas}}\left(\frac{M^{f}_{\rm BH}}{10^{8}\,M_{\odot}}\right)^{0.2}\frac{L}{L_{\rm peak}}\,. \qquad (12)$$

We can use this to estimate the optical luminosity function of quasar hosts by taking our already determined optical/UV merging galaxy luminosity functions and adding the selection criteria appropriate to these galaxies being identified as the hosts of bright optical quasars.

We show in § 3.1 that the median merger optical/UV luminosity is roughly constant in time, but the quasar luminosity can vary by orders of magnitude and spends much of its time at luminosities well below $L_{\rm peak} \sim L_{\rm Edd}(M_{\rm BH})$. Consequently, the observed quasar luminosity is uncorrelated with the host galaxy luminosity. This is discussed further in Hopkins et al. (2005c, 2006b) in the context of the observed lack of correlation between quasar luminosity and black hole mass (e.g., Ho 2002; Heckman et al. 2004; Hao et al. 2005), but similarly explains the observed lack of a correlation between nuclear and host galaxy optical luminosity (Bahcall et al. 1997; McLure et al. 1999; Jahnke & Wisotzki 2003; Hao et al. 2005; Vanden Berk et al. 2006). At the brightest luminosities above the break in the QLF, this is no longer strictly true, as black holes do increasingly tend to be at a high Eddington ratio and near their peak luminosity, and a correlation between nuclear and host luminosity is expected (although at these luminosities measuring host properties is most difficult).

Using our modeling of the quasar and galaxy luminosities during a merger, we can predict the joint distribution in optical quasar and host galaxy luminosity. In Figure 14, we generate a mock sample of ~ 2000 optical "AGN" and plot their quasar and host galaxy *B*-band magnitudes. The procedure by which the mock distribution is generated is described in detail in Hopkins et al. (2006b), but briefly, we consider intervals of $\log(M_{\rm BH})$ from the distribution of relic black hole masses $ri(M_{\rm BH})$ at $z = 0.5$ with $10^{6}\,M_{\rm BH} < L_{\rm peak} < 10^{10}\,M_{\odot}$. For each, we consider the simulations with the nearest $M_{\rm BH}$, and calculate the PDF for their being observed as optical AGN (defined here by $M_{B,\,\rm qso} < -16$ and an obscuring column density $N_H < 10^{22}\,{\rm cm}^{-2}$) with a given AGN and host galaxy *B*-band luminosity (both calculated including attenuation using the methodology in Hopkins et al. (2006b), but adopting the empirical fit to column density distributions as a function of luminosity from Ueda et al. (2003) yields very similar results). From this distribution, we randomly calculate ~ 2000 points in $M_{B,\,\rm qso}$, $M_{B,\,\rm gal}$, which are shown in the figure. We assume $f_{\rm gas} = 0.2$, but this only changes the normalization of $M_{B,\,\rm gal}$ in this distribution. For comparison, the dashed line in the figure shows $L_{B,\,\rm gal} = L_{B,\,\rm qso}$ and the solid line shows $L_{B,\,\rm gal} = 0.1\,L_{B,\,\rm qso}$. These approximately correspond to Eddington ratios of $L \approx 0.1\,L_{\rm Edd}$ and $L \approx L_{\rm Edd}$, respectively. The distribution demonstrates the lack of correlation between quasar and host galaxy luminosity, and agrees well with various observational estimates (e.g., Bahcall et al. 1997; McLure et al. 1999; Jahnke & Wisotzki 2003; Sánchez et al. 2004). Specifically, compare Figure 13 of Vanden Berk et al. 2006, who find a nearly identical distribution considering host galaxy-AGN spectral decomposition of SDSS AGN complete to $L_{g,\,\rm gal} \approx 0.1\,L_{g,\,\rm qso}$ (where the SDSS *g*-band is generally equivalent to *B*-band for our purposes).

For a given $M_{\rm BH}$ (or correlated merging galaxy luminosity), we can calculate from Equation (12) and our scaling of the quasar lifetime as a function of instantaneous and peak luminosities the time spent above some observed quasar *B*-band luminosity limit $L_{B,\,\rm qso}$ and/or some limit in the ratio of quasar to host galaxy optical luminosity $L_{B,\,\rm qso}/L_{B,\,\rm gal}$; i.e. the time

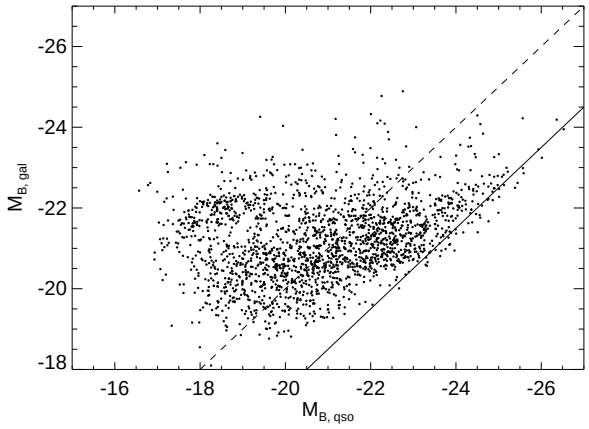

FIG. 14.— Predicted optical *B*-band quasar and host galaxy magnitudes for a mock sample of ~ 2000 optical "AGN" with $L_{\rm peak} > 10^{9}\,L_{\odot}$, at redshift $z = 0.5$. Dashed line shows $L_{B,\,\rm gal} = L_{B,\,\rm qso}$ ($L_{\rm QSO} \approx 0.1\,L_{\rm Edd}$), solid line $L_{B,\,\rm gal} = 0.1\,L_{B,\,\rm qso}$ ($L_{\rm QSO} \approx L_{\rm Edd}$). Quasar and host luminosities are uncorrelated except at the brightest luminosities where systems are generally near-Eddington, as observed (e.g., Hao et al. 2005).

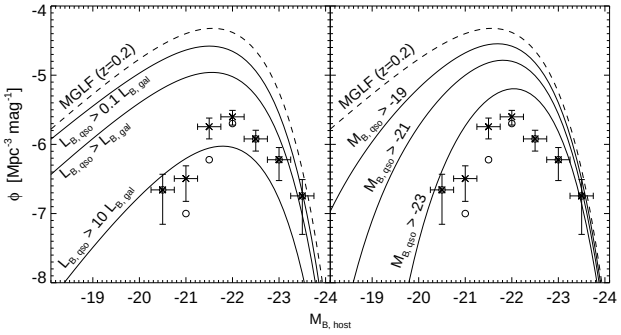

FIG. 15.— Predicted *B*-band HGLF of optical quasars at $z = 0.2$. Dashed line shows the full best-fit *B*-band MGLF (assuming $\alpha = 0.5$), solid lines show the HGLF requiring an observed *B*-band quasar luminosity above a given fraction of the host galaxy luminosity (left panel, as labeled) or requiring an observed *B*-band quasar magnitude above some fixed limit (right panel, as labeled). Points show the observational estimate of Hamilton et al. (2002) (requiring $M_{V,\,\rm qso} < -23$, open circles) at $z \sim 0-0.4$, rescaled to typical *B*-band host luminosities following Bahcall et al. (1997) and Vanden Berk et al. (2006). Although these quasars are not necessarily predicted to be observed in an obvious merger stage, their host luminosity function is a subset of the MGLF, selected at a different merger stage.

during which we estimate the merging galaxy can be identified as a traditional optical or broad-line AGN host galaxy. Figure 15 shows this calculation assuming different selection criteria in determining the HGLF. In the left panel, we show the MGLF at $z = 0.2$, determined from the $z = 0.2$ hard X-ray QLF of Ueda et al. (2003) as the dashed line. For clarity, we do not show the uncertainty in this prediction, but adopt the best-fit assuming $\alpha = -0.5$ and $f_{\rm gas} = 0.2$; the uncertainty in the plotted MGLF can be seen in the upper and lower middle panels of Figure 7. As solid lines, we then show the HGLF, i.e. the MGLF given some selection criteria for the quasar and host galaxy B-band luminosity, namely $L_{B,\,\rm qso} > 0.1\,L_{B,\,\rm gal}$, $L_{B,\,\rm qso} > L_{B,\,\rm gal}$, and $L_{B,\,\rm qso} > 10\,L_{B,\,\rm gal}$, as labeled. In the right panel, we show the same, but instead imposing the B-band quasar magnitude limits $M_{B,\,\rm qso} < -19$, $M_{B,\,\rm qso} < -21$, and $M_{B,\,\rm qso} < -23$, as labeled. In each, the observationally estimated optical quasar HGLF of Hamilton et al. (2002) is plotted, which is composed of quasars primarily of optical magnitude $M_B < -23$ (crosses with error bars; open circles show the inferred luminosity function applying a strict $M_V < -23$ magnitude cut). There is some uncertainty in the absolute normalization of the host galaxy luminosities, discussed in Hamilton et al. (2002); therefore we rescale their V-band host galaxy luminosities to the B-band using the calibrations of the overlapping samples in Bahcall et al. (1997); McLure et al. (1999), which gives a peak in the HGLF similar to that observed in e.g. Bahcall et al. (1997) and the much larger sample of Vanden Berk et al. (2006) at $M_B \approx -22$.

In any case, when we require that a bright optical quasar ($M_B < -23$) be observable as such, we find good agreement between our predicted HGLF and the observed distribution of host galaxy luminosities. There are several uncertainties in this comparison: for example, the normalization and absolute host magnitudes of the observed sample may be biased if the quasar light is not perfectly subtracted, our prediction only loosely estimates the full distribution of dust obscuration as a function of time (see Hopkins et al. 2006b for a discussion; the key point is that by $M_B < -23$, a more accurate prediction from our simulations of the HGLF may be up to a factor ~ 2 lower), and as shown in Figure 7 the uncertainties in the initial MGLF (which propagate linearly into the HGLF) are large. For these reasons, the slight discrepancy in normalization between our prediction and the observations is not significant. Also, note that the appearance in Figure 15 that all bright mergers host optical quasars is an artifact of how steeply the Schechter function falls off – even at the brightest luminosities, there can be a factor $\sim 2-10$ difference between the MGLF and $M_B < -23$ HGLF prediction.

However, despite these uncertainties, the key qualitative point is clear – the quasar HGLF can be understood as a subset of the MGLF, with the appropriate though more sophisticated selection criteria applied as only those mergers during (or after) the "blowout" phase will be identified. The characteristic magnitude, relative normalization, and narrow width of the HGLF are explained in our modeling, demonstrating that this luminosity function is self-consistent with both the QLF and MGLF in our interpretation of quasar fueling. Observations of e.g. the fraction of mergers with optical AGN (e.g., Sánchez et al. 2005), although traditionally more difficult than observations of the fraction of AGN in mergers, also suggest a similar fraction of mergers hosting optical AGN to that we predict for the appropriate luminosity limits in Figure 15. Although we have only shown this at one redshift, where most of the observations have been made, the qualitative result is the same regardless of the redshift (or e.g. value of $f_{\rm gas}$ or α) chosen.

This does not imply that all quasar host galaxies will be visible as mergers or interacting systems, although the low-redshift sample of Bahcall et al. (1997) indeed identifies the vast majority as such. Generally, the "blowout" phase in our simulations follows the final coalescence of the black holes, meaning that tidal tails and other evidence of a recent merger should in principle be evident, but at higher redshift surface brightness dimming will make these features nearly impossible to observe. Moreover, once the blowout begins, star formation is terminated and the host galaxy rapidly begins to redden, and extended tidal features will fade in ~ 1 Gyr.

The HGLF distribution we predict is consistent with observed properties of lower-luminosity AGN host galaxies. For example, Kauffmann et al. (2003a) study the host galaxies of $\sim 20,000$ SDSS narrow line, relatively low-luminosity AGN at $z < 0.3$ and find that a large fraction of these objects correspond to what we expect from simulations for post-"blowout" objects with rapidly declining accretion rates in relaxing, rapidly reddening systems (see e.g. Hopkins et al. [2006a] for a description of the falloff in AGN luminosity as the merger relaxes). These objects reside in massive spheroids, with properties of "normal" ellipticals except for young stellar populations and evidence of starbursts in the past $\sim 1-2$ Gyr, with a sizable fraction ($\sim 30\%$) of especially the brightest objects showing obvious evidence of interaction and/or recent mergers. Similar results are also found for e.g. the AGN host population in GEMS (Sánchez et al. 2004) and radio loud quasars (Sánchez & González-Serrano 2003), although these may be preferentially at relatively low accretion rates (e.g., Ho 2002; Hopkins, Narayan, & Hernquist 2006).

8. DISCUSSION

We have used simulations of galaxy mergers which account for star formation, metal enrichment, radiative cooling, supernova feedback and pressurization of a multi-phase interstellar medium, and black hole growth and feedback, to relate the distribution of observed quasar properties and its evolution with redshift to the distributions of merging galaxy properties, including their luminosity and mass functions, characteristic gas fractions, and contribution to the star formation rate density of the Universe. Our simulations span a wide range of initial and final conditions, varying virial velocities, initial gas fractions, masses, orbital parameters, initial black hole masses, ISM gas equations of state, redshifts, and galaxy mass ratios. Our modeling allows us to self-consistently map between the merging galaxy and quasar distributions in a physically motivated manner without invoking tunable cosmological distributions and enables predictions of many properties of merging galaxies at different redshifts.

We find that:

• The joint scaling of dust obscuration and star formation with gas density yields quite flat lightcurves in the optical/UV, allowing us to provide a simple parameterization of the probability for observing a particular merger at a certain luminosity. To enable future comparison with observations, we provide fits from our simulations to infer the distribution of observed luminosities in different bands as a function of the stellar mass formed in mergers, total stellar mass, or final black hole mass of the merging systems (Table 1). Our simulations allow us to determine color and mass-to-light ratio distributions of mergers, which we find to be in good agreement with those observed, and self-consistently map between e.g. ob-

served merger luminosity functions in the near IR, optical, and UV, star formation rate distributions, mass functions, and mass or luminosity-dependent merger rates.

• We consider in detail observed merger luminosity functions in *K*-band at $z < 0.2$ (Xu et al. 2004) and 280 nm at $z = 0.7$ (Wolf et al. 2005), and mass functions at $z \sim 0.4,\ 0.7,\ 1.2$ (Bundy et al. 2005a,b). We use our simulations to map them to a quasar luminosity function at each redshift, and find that the predicted quasar luminosity functions agree with those observed by e.g. Ueda et al. (2003). Conversely, we invert this procedure, predicting the merger luminosity function from the observed quasar luminosity function, and again find agreement, although the predictions are significantly less well-constrained in this direction. Both distributions are self-consistent (each predicts the other) and can be used to predict merger rates and the rate of formation of quasars or spheroids as a function of that luminosity, mass and redshift.

Although merger mass functions are not yet well determined above these redshifts, the demonstration in Hopkins et al. (2006d) that the characteristic masses of observed mergers, the "quenching" or "transition" mass where elliptical galaxies begin to dominate the total galaxy population, and the characteristic mass of quasars (at the observed QLF break) all trace one another over the range $0 < z \lesssim 3$ further suggests that this mapping is valid at high redshift. We extend our predictions of merger luminosity functions by using the observed QLF to predict the merger luminosity density in *K* and *B*-bands from $z = 0-6$ with small factors ~ 2 uncertainties. The prediction agrees with existing observations at $z \lesssim 3$ (Brinchmann et al. 1998; Toledo et al. 1999; Conselice et al. 2003, 2005; Xu et al. 2004; Bundy et al. 2005a,b), but the present observational uncertainties are large. Future measurements of the mass or luminosity density in mergers will provide a critical test of this model and the association between mergers and quasar triggering at all redshifts.

•We compare this relation of merger and quasar distributions to that inferred if quasars turn "on/off" in step-function fashion or follow exponential lightcurves, and find that the observations rule out such scenarios at $\gtrsim 99.9\%$ confidence, even if we allow the quasar lifetime to vary freely to produce the best fit. This can be determined entirely from the observed *shapes* of the QLF and MGLF, independent of selection efficiencies, gas fractions, or other cosmological properties; it would require a $\gtrsim 4-6\sigma$ change in the observed shape to reverse this conclusion. Any comparison of merger rates or merger distributions and quasar activity must account for complex quasar lightcurves and the non-trivial nature of quasar lifetimes which vary as a function of both instantaneous and peak luminosity.

•We use the QLF to predict the distribution of star formation rates (SFRF) at various redshifts, and subsequently the SFR density in mergers as a function of redshift from $z = 0-6$. Comparison of these predictions with measurements, which currently exist at $z \lesssim 1$ (Brinchmann et al. 1998; Menanteau et al. 2001, 2006; Bell et al. 2005), shows good agreement, and suggests that the QLF can provide a new, powerful, and independent probe of the SFR density in the Universe driven by mergers. At redshifts $z \lesssim 4$, this allows us to predict the SFR density caused by mergers to a factor $\sim 1.5-2$ accuracy, with the primary systematic uncertainty being weak constraints on typical gas fractions of disks at low redshift $z \lesssim 1$. At $z > 4$, future improvements in constraints on the QLF break luminosity will enable similar predictions, without a large uncertainty in gas fractions, as gas-rich systems are expected at these high redshifts. Thus, quasar measurements can constrain the SFR density triggered by mergers at high redshifts and at the end of the reionization epoch, where attempts to measure morphological properties of galaxies and determine this quantity directly are not likely to be possible in the near future. This also provides a prediction of the total rate at which mass is moved from the blue (disk) sequence to the red (spheroid) sequence, independent of gas fraction, as analyzed in detail in Hopkins et al. (2006c).

We find that the SFR density triggered in mergers is small at low redshift: $\sim 1\%$ of the total SFR density at $z \sim 0$. This fraction of the SFR density rises to a substantial, but not dominant $\sim 40\%$ (upper limit 60%) at $z \sim 2-3$, and remains approximately constant at higher redshift (relative to the total SFR density from Hopkins & Beacom (2006)). Given the low level of star formation in remnant ellipticals, the dominant contribution to the SFR density (especially at $z \lesssim 2$) must come from late-type spiral or irregular galaxies.

• We predict the joint distribution of quasar and host galaxy luminosities in good agreement with observations (Bahcall et al. 1997; McLure et al. 1999; Vanden Berk et al. 2006). The lack of a correlation between quasar and host galaxy luminosities (especially at low quasar luminosity; Bahcall et al. 1997; McLure et al. 1999; Ho 2002; Jahnke & Wisotzki 2003; Heckman et al. 2004; Hao et al. 2005; Vanden Berk et al. 2006) is a natural consequence of the nearly constant optical/UV merger light curves we discuss above while quasar luminosities change by orders of magnitude during a merger.

We predict the quasar host galaxy luminosity function (HGLF) from either the observed QLF or merging galaxy luminosity function (MGLF) at any given redshift. We find that the HGLF has a similar shape to the MGLF in a given band, but becomes increasingly peaked about M_* as the minimum optical quasar luminosity or minimum ratio of optical quasar to optical host galaxy luminosity is increased. For a given minimum quasar optical luminosity, e.g. $M_B < -23$, we find good agreement between the observed HGLF (Bahcall et al. 1997; Hamilton et al. 2002; Vanden Berk et al. 2006) and our prediction from the observed MGLF of Xu et al. (2004) or QLF of Ueda et al. (2003). The observed shape, normalization, and break/turnover luminosity in the quasar HGLF is a natural consequence of its being a subset of the MGLF, with e.g. a break at approximately the same luminosity (so long as the luminosity limit of the quasars in the sample is not so high as to exclude typical $\sim M_*$ hosts). This does not mean that quasar hosts will be obvious mergers, as the bright optical phase of quasar activity is associated with the "blowout" phase following the final coalescence, in which difficult to observe, rapidly fading tidal features may represent the only morphological merger signature.

We have demonstrated that the statistics and distributions of merging galaxy and quasar populations are self-consistent and can be used to predict one another in the context of the merger hypothesis. Coupled with the analysis of quasar properties in Hopkins et al. (2005a-d, 2006a,b), remnant red-sequence elliptical galaxies in Hopkins et al. (2006c), and the co-evolution of the "transition" mass and merger and quasar masses in Hopkins et al. (2006d), the modeling presented here unifies the populations of multiple relevant merger stages. The number of observed mergers accounts for the bright quasar population as well as the observed buildup in the mass of the elliptical / red-sequence galaxy population, and vice versa. *There is no room for a large fraction of gas-*

rich mergers which do not produce a bright quasar phase and remnant, reddening elliptical, nor is there room for a large fraction of bright quasars or elliptical galaxies which are not formed in gas-rich mergers.

This allows us to make a wide range of predictions and provides a critical test of the hypothesis that starbursts, quasars, and elliptical galaxies are linked through the process of gas-rich mergers, a test which is complimentary and equally important to measurements of the individual photometric and kinematic properties and correlations of mergers and merger remnants (e.g., their profiles, metal enrichment, phase space densities, fundamental plane and $M_{\rm BH}-\sigma$ relations: Lake & Dressler 1986; Doyon et al. 1994; Oliva et al. 1995; Shier & Fischer 1998; James et al. 1999; Genzel et al. 2001; Rothberg & Joseph 2004, 2006) and comparison of these remnants to detailed simulations (e.g., Barnes & Hernquist 1992; Hernquist 1993a; Hernquist et al. 1993; Springel et al. 2005a; Cox et al. 2005; Robertson et al. 2005a, 2006b).

This does not mean, of course, that ellipticals never evolve via dry (gas-poor, spheroid-spheroid) mergers (see, e.g., Bell et al. 2006a; van Dokkum 2005), as such mergers only modify a necessarily pre-existing population of ellipticals (see also Hopkins et al. (2006c) for a calculation of the effects of such processes on observed elliptical distributions). This also does not imply that all AGN activity is associated with gas-rich mergers, as there can be a substantial contribution to low-luminosity AGN from activity triggered in quiescent spirals (for a detailed comparison, see Hopkins & Hernquist 2006), as well as the large amount of quiescent, low-level activity in relaxed ellipticals which we predict (and account for) many dynamical times after the spheroid-forming merger as the quasar lightcurve decays (Hopkins et al. 2006b).

Our modeling makes predictions that can be used to test our underlying theory. For example, mergers at high redshifts should involve galaxies that are, on average, more gas-rich than local spirals (our preliminary comparison, for example, favors an exponentially declining $f_{\rm gas}$ over $\sim$ a few Gyr). Preliminary evidence from Erb et al. (2006) indicates that galaxies at redshift $z\approx 2$ do, indeed, have large gas fractions $f_{\rm gas}\sim 0.5$, with some approaching $f_{\rm gas}\sim 0.8-0.9$, but future observatories such as ALMA should be able to measure this accurately. The connection between merger-driven star formation and quasar activity can also be used to test the correlation between our predicted SFR distributions and quasar peak luminosity. This should be possible with improved observations of quasar hosts in relaxed, post-merger systems which can be used to determine their individual star formation histories (e.g., Kauffmann et al. 2003a), as well as measurements of star formation in obscured, lower-luminosity merger phases, possibly associated with IR-bright Type 2 quasar activity (e.g., C. Hao et al. 2005; Kim et al. 2006) and strongly reddened optical quasars (e.g., Urrutia et al. 2005).

Mergers of gas-rich spirals will imprint structure into the remnants that may be difficult to account for otherwise (see e.g., Robertson et al. 2006b; Cox et al. 2005). The starburst population left behind will characteristically modify the central light profiles and kinematics of merger remnants (e.g. Mihos & Hernquist 1994b; Hernquist & Barnes 1991), possibly explaining the central excesses of light seen in merging systems (e.g. Rothberg & Joseph 2004, 2006), and the presence of kinematic subsystems in ellipticals. This can be tested in detail by comparing predictions for metallicity and color gradients and orbital distributions with observations.

More subtle may be the shells, ripples, loops and other fine structures seen around many relaxed ellipticals (see, e.g. Schweizer 1998) that require a source of dynamically cold stellar material and are hence a natural consequence of major mergers involving disk galaxies (e.g. Hernquist & Spergel 1992), but do *not* form in major mergers between hot stellar systems (e.g. Hernquist & Quinn 1988). A measurement of the rate of occurrence of fine structure in red galaxies with redshift would further constrain the importance of mergers involving disk galaxies to the formation of ellipticals (Bell et al. 2006a; van Dokkum 2005).

We use our simulations to develop a formalism to derive the relations between the various populations we have studied in a manner robust against different cosmological distributions which are poorly constrained and often tuned to reproduce observations. However, this also means that we cannot constrain certain cosmological distributions. For example, we find that the distribution of observed luminosities of a merger is robust when expressed as a function of the final stellar mass or total stellar mass formed in the merger. This enables us to map the MGLF to a merger mass function, but does not allow us to consider the relative contribution of mergers with e.g. different initial mass ratios, ISM equations of state, or star formation histories. It will be interesting to see whether cosmological simulations yield the distributions of merger statistics that we have derived from quasar, merger, and elliptical galaxy observations. Coupling such cosmological descriptions with our detailed modeling of the complex star formation and black hole growth histories in mergers enables an a priori theoretical prediction of the wide array of phenomena we have demonstrated are linked through gas-rich galaxy mergers.

We thank E. Bell and C. Wolf for providing their data in electronic form. This work was supported in part by NSF grants ACI 96-19019, AST 00-71019, AST 02-06299, and AST 03-07690, and NASA ATP grants NAG5-12140, NAG5-13292, and NAG5-13381. The simulations were performed at the Center for Parallel Astrophysical Computing at the Harvard-Smithsonian Center for Astrophysics. RSS thanks the Institute for Theory and Computation at the Harvard-Smithsonian Center for Astrophysics for hospitality.

REFERENCES

Alexander, D. M., et al. 2005a, Nature, 434, 738
Alexander, D. M., Bauer, F. E., Chapman, S. C., Smail, I., Blain, A. W., Brandt, W. N., & Ivison, R. J. 2005b, ApJ, 632, 736
Allen, D.A., Roche, P.F. & Norris, R.P. 1985, MNRAS, 213, 67p
Armus, L., Heckman, T.M. & Miley, G. 1987, AJ, 94, 831
Arribas, S., Bushouse, H., Lucas, R. A., Colina, L., & Borne, K. D. 2004, AJ, 127, 2522
Bahcall, J.N., Kirhakos, S. & Schneider, D.P. 1994, ApJ, 435, L11
Bahcall, J.N., Kirhakos, S. & Schneider, D.P. 1995, ApJ, 450, 486
Bahcall, J. N., Kirhakos, S., Saxe, D. H., & Schneider, D. P. 1997, ApJ, 479, 642
Barnes, J.E. 1998, in Galaxies: Interactions and Induced Star Formation, eds. D. Friedli, L. Martinet & D. Pfenniger (Springer-Verlag, Berlin), p. 275
Barnes, J. E. & Hernquist, L. 1991, ApJ, 370, L65
Barnes, J. E. & Hernquist, L. 1992, ARA&A, 30, 705
Barnes, J. E. & Hernquist, L. 1996, ApJ, 471, 115
Bauer, A. E., Drory, N., Hill, G. J., & Feulner, G. 2005, ApJ, 621, L89
Baugh, C. M., Lacey, C. G., Frenk, C. S., Granato, G. L., Silva, L., Bressan, A., Benson, A. J., & Cole, S. 2005, MNRAS, 356, 1191

Bell, E. F., McIntosh, D. H., Katz, N., & Weinberg, M. D. 2003, ApJS, 149, 289
Bell, E. F., et al. 2005, ApJ, 625, 23
Bell, E. F., et al. 2006a, ApJ, 640, 241
Bell, E. F., Phleps, S., Somerville, R. S., Wolf, C., Borch, A., & Meisenheimer, K. 2006b, ApJ, in press [astro-ph/0602038]
Borch, A., et al. 2006, A&A, in press, astro-ph/0604405
Borys, C., Smail, I., Chapman, S. C., Blain, A. W., Alexander, D. M., & Ivison, R. J. 2005, ApJ, 635, 853
Bouchet, P., Lequeux, J., Maurice, E., Prevot, L., & Prevot-Burnichon, M. L. 1985, A&A, 149, 330
Brinchmann, J., et al. 1998, ApJ, 499, 112
Brotherton, M. S., et al. 1999, ApJ, 520, L87
Brotherton, M. S., Grabelsky, M., Canalizo, G., van Breugel, W., Filippenko, A. V., Croom, S., Boyle, B., & Shanks, T. 2002, PASP, 114, 593
Bruzual, G. & Charlot, S. 2003, MNRAS, 344, 1000
Bullock, J. S., Kolatt, T. S., Sigad, Y., Somerville, R. S., Kravtsov, A. V., Klypin, A. A., Primack, J. R., & Dekel, A. 2001, MNRAS, 321, 559
Bundy, K., Fukugita, M., Ellis, R. S., Kodama, T., & Conselice, C. J. 2004, ApJ, 601, L123
Bundy, K., Ellis, R. S., & Conselice, C. J. 2005a, ApJ, 625, 621
Bundy, K., et al. 2005b, ApJ, in press [astro-ph/0512465]
Burkley, J. M., et al. 1994, ApJ, 429, L13
Burstein, D., Davies, R. L., Dressler, A., Faber, S. M., & Lynden-Bell, D. 1988, ASSL Vol. 141: Towards Understanding Galaxies at Large Redshift, 17
Busha, M. T., Evrard, A. E., Adams, F. C., & Wechsler, R. H. 2005, MNRAS, 363, L11
Calzetti, D., Kinney, A. L., & Storchi-Bergmann, T. 1994, ApJ, 429, 582
Canalizo, G., Stockton, A., Brotherton, M. S., & van Breugel, W. 2000, AJ, 119, 59
Canalizo, G. & Stockton, A. 2001, ApJ, 555,719
Carlberg, R. G. 1986, ApJ, 310, 593
Carlberg, R. G., Pritchet, C. J., & Infante, L. 1994, ApJ, 435, 540
Cen, R., Miralda-Escudé, J., Ostriker, J. P., & Rauch, M. 1994, ApJ, 437, L9
Chakrabarti, S., Cox, T.J., Hernquist, L., Hopkins, P., Robertson, B., Springel, V., & Di Matteo, T., 2006, ApJ, submitted [astro-ph/0605652]
Cole, S., Lacey, C. G., Baugh, C. M., & Frenk, C. S. 2000, MNRAS, 319, 168
Cole, S., et al. 2001, MNRAS, 326, 255
Conselice, C. J., Bershady, M. A., Dickinson, M., & Papovich, C. 2003, AJ, 126, 1183
Conselice, C. J., Blackburne, J. A., & Papovich, C. 2005, ApJ, 620, 564
Cox, T. J., Di Matteo, T., Hernquist, L., Hopkins, P. F., Robertson, B., & Springel, V. 2005, ApJ, in press [astro-ph/0504156]
Croft, R.A.C., Weinberg, D.H., Katz, N. & Hernquist, L. 1998, ApJ, 495, 44
Croft, R.A.C., Weinberg, D.H., Pettini, M., Hernquist, L. & Katz, N. 1999, ApJ, 520, 1
Croft, R.A.C., Weinberg, D.H., Bolte, M., Burles, S. Hernquist, L., Katz, N., Kirkman, D., & Tytler, D. 2002, ApJ, 581, 20
Croom, S. M., Smith, R. J., Boyle, B. J., Shanks, T., Miller, L., Outram, P. J., & Loaring, N. S. 2004, MNRAS, 349, 1397
Cross, N. J. G., et al. 2004, AJ, 128, 1990
Croton, D. J., et al. 2006, MNRAS, 365, 11
Daddi, E., et al. 2004, ApJ, 600, L127
Dasyra, K. M., et al. 2006, ApJ, 638, 745
Davé, R., Hernquist, L., Katz, N. & Weinberg, D.H. 1999, ApJ, 511, 521
de Mello, D. F., Wadadekar, Y., Dahlen, T., Casertano, S., & Gardner, J. P. 2006, AJ, 131, 216
Di Matteo, T., Springel, V., & Hernquist, L. 2005, Nature, 433, 604
Doyon, R., Wells, M., Wright, G. S., Joseph, R. D., Nadeau, D., & James, P. A. 1994, ApJ, 437, L23
Dunlop, J. S., McLure, R. J., Kukula, M. J., Baum, S. A., O'Dea, C. P., & Hughes, D. H. 2003, MNRAS, 340, 1095
Ellison, S. L., Hall, P. B., & Lira, P. 2005, AJ, 130, 1345
Elvis, M., et al. 1994, ApJS, 95, 1
Erb, D. K., Steidel, C. C., Shapley, A. E., Pettini, M., Reddy, N. A., & Adelberger, K. L. 2006, ApJ, in press [astro-ph/0604041]
Faber, S. M., Trager, S. C., Gonzalez, J. J., & Worthey, G. 1995, IAU Symp. 164: Stellar Populations, 164, 249
Falomo, R., Kotilainen, J., & Treves, A. 2001, ApJ, 547, 124
Ferrarese, L. & Merritt, D. 2000, ApJ, 539, L9
Feulner, G., Gabasch, A., Salvato, M., Drory, N., Hopp, U., & Bender, R. 2005, ApJ, 633, L9
Floyd, D. J. E., Kukula, M. J., Dunlop, J. S., McLure, R. J., Miller, L., Percival, W. J., Baum, S. A., & O'Dea, C. P. 2004, MNRAS, 355, 196
Franceschini, A. et al. 2006, A&A, in press [astro-ph/0601003]
Gebhardt, K., Bender, R., Bower, G. et al. 2000, ApJ, 539, L13
George, I. M., Turner, T. J., Netzer, H., Nandra, K., Mushotzky, R. F., & Yaqoob, T. 1998, ApJS, 114, 73
Genzel, R., et al. 1998, ApJ, 498, 579
Genzel, R., Tacconi, L. J., Rigopoulou, D., Lutz, D., & Tecza, M. 2001, ApJ, 563, 527
Gerssen, J. et al. 2004, AJ, 127, 75
Granato, G. L., De Zotti, G., Silva, L., Bressan, A., & Danese, L. 2004, ApJ, 600, 580
Green, P. J., et al. 1995, ApJ, 450, 51
Gunn, J.E. 1987, in Nearly Normal Galaxies, ed. S. Faber (Springer-Verlag; New York), p. 455
Haiman, Z., & Loeb, A. 1998, ApJ, 503, 505
Haiman, Z., & Menou, K. 2000, ApJ, 531, 42
Haiman, Z., Quataert, E., & Bower, G. C. 2004, ApJ, 612, 698
Hamilton, T. S., Casertano, S., & Turnshek, D. A. 2002, ApJ, 576, 61
Hammer, F., Flores, H., Elbaz, D., Zheng, X. Z., Liang, Y. C., & Cesarsky, C. 2005, A&A, 430, 115
Hao, L., et al. 2005, AJ, 129, 1795
Hao, C. N., Xia, X. Y., Mao, S., Wu, H., & Deng, Z. G. 2005, ApJ, 625, 78
Häring, N., & Rix, H.-W. 2004, ApJ, 604, L89
Hasinger, G., Miyaji, T., & Schmidt, M. 2005, A&A, 441, 417
Heckman, T. M., Bothun, G. D., Balick, B., & Smith, E. P. 1984, AJ, 89, 958
Heckman, T. M., Kauffmann, G., Brinchmann, J., Charlot, S., Tremonti, C., & White, S. D. M. 2004, ApJ, 613, 109
Hernquist, L. 1990, ApJ, 356, 359
Hernquist, L. 1992, ApJ, 400, 460
Hernquist, L. 1993a, ApJ, 409, 548
Hernquist, L. 1993b, ApJ, 404, 717
Hernquist, L. & Barnes, J.E. 1991, Nature, 354, 210
Hernquist, L., & Mihos, J. C. 1995, ApJ, 448, 41
Hernquist, L. & Quinn, P.J. 1988, ApJ, 331, 682
Hernquist, L. & Spergel, D.N. 1992, ApJ, 399, L117
Hernquist, L., Spergel, D.N. & Heyl, J.S. 1993, ApJ, 416, 415
Hernquist, L., Katz, N., Weinberg, D. & Miralda-Escudé, J. 1996, ApJ, 457, L51
Hernquist, L., & Springel, V. 2003, MNRAS, 341, 1253
Ho, L. C. 2002, ApJ, 564, 120
Hoekstra, H., Hsieh, B. C., Yee, H. K. C., Lin, H., & Gladders, M. D. 2005, ApJ, 635, 73
Hopkins, A. M. 2004, ApJ, 615, 209
Hopkins, A. M., & Beacom, J. F. 2006, ApJ, in press [astro-ph/0601463]
Hopkins, P. F., Bundy, K., Hernquist, L., Ellis, R. S., 2006d, ApJ, submitted [astro-ph/0601621]
Hopkins, P. F., & Hernquist, L. 2006, ApJS, in press [astro-ph/0603180]
Hopkins, P. F., Hernquist, L., Martini, P., Cox, T. J., Robertson, B., Di Matteo, T., & Springel, V. 2005a, ApJ, 625, L71
Hopkins, P. F., Hernquist, L., Cox, T. J., Robertson, B., Di Matteo, T., Martini, P., & Springel, V. 2005b, ApJ, 630, 705
Hopkins, P. F., Hernquist, L., Cox, T. J., Robertson, B., Di Matteo, T., & Springel, V. 2005c, ApJ, 630, 716
Hopkins, P. F., Hernquist, L., Cox, T. J., Robertson, B., Di Matteo, T., & Springel, V. 2005d, ApJ, 632, 81
Hopkins, P. F., Hernquist, L., Cox, T. J., Robertson, B., Di Matteo, T., & Springel, V. 2006a, ApJ, 639, 700
Hopkins, P. F., Hernquist, L., Cox, T. J., Robertson, B., Di Matteo, T., & Springel, V. 2006b, ApJS, 163, 1
Hopkins, P. F., Hernquist, L., Cox, T. J., Robertson, B., & Springel, V. 2006c, ApJS, 163, 50
Hopkins, P. F., Narayan, R., Hernquist, L., 2006, ApJ, in press [astro-ph/0510369]
Hopkins, P. F., Richards, G.T., & Hernquist, L., 2006, ApJ, submitted [astro-ph/0605678]
Hopkins, P. F., Strauss, M. A., Hall, P. B., Richards, G. T., Cooper, A. S., Schneider, D. P., Vanden Berk, D. E., Jester, S., Brinkmann, J., & Szokoly, G. P. 2004, AJ, 128, 1112
Hui, L., Burles, S., Seljak, U., Rutledge, R.E., Magnier, E. & Tytler, D. 2001, ApJ, 552, 15
Hutchings, J. B., & Neff, S. G. 1992, AJ, 104, 1
Jahnke, K., & Wisotzki, L. 2003, MNRAS, 346, 304
James, P., Bate, C., Wells, M., Wright, G., & Doyon, R. 1999, MNRAS, 309, 585
Jogee, S. 2005, in AGN Physics on All Scales, LNP Volume, eds. D. Alloin, R. Johnson & P. Lira (Springer: Berlin), Ch. 6, [astro-ph/0408383]
Jonsson, P., Cox, T. J., Primack, J. R., & Somerville, R. S. 2006, ApJ, 637, 255
Jørgensen, I. 1997, MNRAS, 288, 161
Joseph, R.D. & Wright, G.S. 1985, MNRAS, 214, 87

Katz, N., Weinberg, D.H., Hernquist, L. & Miralda-Escudé, J. 1996a, ApJ, 457, L57
Katz, N., Weinberg, D.H. & Hernquist, L. 1996b, ApJS, 105, 19
Kauffmann, G., et al. 2003a, MNRAS, 346, 1055
Kauffmann, G., et al. 2003b, MNRAS, 341, 54
Kauffmann, G. & Haehnelt, M. 2000, MNRAS, 311, 576
Keel, W. C., & Wu, W. 1995, AJ, 110, 129
Kennicutt, R. C. 1998, ApJ, 498, 541
Kim, M., Ho, L. C., & Im, M. 2006, ApJ, in press [astro-ph/0601316]
Kleinmann, S.G. et al. 1988, ApJ, 328, 161
Komossa, S., Burwitz, V., Hasinger, G., Predehl, P., Kaastra, J. S., & Ikebe, Y. 2003, ApJ, 582, L15
Kormendy, J. & Richstone, D. 1995, ARA&A, 33, 581
Kormendy, J. & Gebhardt, K. 2001, in AIP Conf. Proc. 586: 20th Texas Symposium on Relativistic Astrophysics, 363
Kuntschner, H. 2000, MNRAS, 315, 184
La Franca, F., et al. 2005, ApJ, 635, 864
Lake, G. 1989, AJ, 97, 1312
Lake, G., & Dressler, A. 1986, ApJ, 310, 605
Le Fèvre, O., et al. 2000, MNRAS, 311, 565
Le Floc'h, E., et al. 2005, ApJ, 632, 169
Leitherer, C., et al. 1999, ApJS, 123, 3
Li, Y., Mac Low, M.-M., & Klessen, R. S. 2005, ApJ, 626, 823
Li, Y., Mac Low, M.-M., & Klessen, R. S. 2006, ApJ, 639, 879
Lidz, A., Hopkins, P. F., Cox, T. J., Hernquist, L., & Robertson, B. 2006, ApJ, 641, 41
Lin, L., et al. 2004, ApJ, 617, L9
Lonsdale, C., Farrah, D., & Smith, H. 2006, in "Astrophysics Update 2". Ed. John W. Mason, Springer/Praxis books, [astro-ph/0603031]
Lotz, J. M., Primack, J., & Madau, P. 2004, AJ, 128, 163
Lotz, J. M., Madau, P., Giavalisco, M., Primack, J., & Ferguson, H. C. 2006, ApJ, 636, 592
Magdziarz, P., & Zdziarski, A. A. 1995, MNRAS, 273, 837
Magorrian, J. et al. 1998, AJ, 115, 2285
Marconi, A., Risaliti, G., Gilli, R., Hunt, L. K., Maiolino, R., & Salvati, M. 2004, MNRAS, 351, 169
Marconi, A., & Hunt, L.K. 2003, ApJ, 589, L21
Martin, C. L., & Kennicutt, R. C. 2001, ApJ, 555, 301
Martini, P. 2004, in Carnegie Obs. Astrophys. Ser. 1, Coevolution of Black Holes and Galaxies, ed. L.C. Ho (Cambridge: Cambridge Univ. Press), 170
Max, C. E., Canalizo, G., Macintosh, B. A., Raschke, L., Whysong, D., Antonucci, R., & Schneider, G. 2005, ApJ, 621, 738
McDonald, P., Miralda-Escudé, J., Rauch, M., Sargent, W.L., Barlow, T.A., Cen, R. & Ostriker, J.P. 2000, ApJ, 543, 1
McDonald, P., et al. 2006, ApJS, 163, 80
McLure, R. J., Kukula, M. J., Dunlop, J. S., Baum, S. A., O'Dea, C. P., & Hughes, D. H. 1999, MNRAS, 308, 377
Melnick, J. & Mirabel, I.F. 1990, A&A, 231, L9
Menanteau, F., Abraham, R. G., & Ellis, R. S. 2001, MNRAS, 322, 1
Menanteau, F., Ford, H. C., Motta, V., Benítez, N., Martel, A. R., Blakeslee, J. P., & Infante, L. 2006, AJ, 131, 208
Mihos, J. C., & Hernquist, L. 1994a, ApJ, 425, L13
Mihos, J. C., & Hernquist, L. 1994b, ApJ, 437, L47
Mihos, J. C., & Hernquist, L. 1996, ApJ, 464, 641
Miyaji, T., Hasinger, G., & Schmidt, M. 2001, A&A, 369, 49
Narayanan, D., et al. 2006, ApJ, in press [astro-ph/0604074]
Navarro J. F., Frenk C. S., White S. D. M., 1996, ApJ, 462, 563
Oliva, E., Origlia, L., Kotilainen, J. K., & Moorwood, A. F. M. 1995, A&A, 301, 55
O'Shea, B. W., Nagamine, K., Springel, V., Hernquist, L., & Norman, M. L. 2005, ApJS, 160, 1
Pannella, M., Hopp, U., Saglia, R. P., Bender, R., Drory, N., Salvato, M., Gabasch, A., & Feulner, G. 2006, ApJ, 639, L1
Papovich, C., et al. 2006, ApJ, 640, 92
Patton, D. R., et al. 1997, ApJ, 475, 29
Patton, D. R., et al. 2000, ApJ, 536, 153
Patton, D. R., et al. 2002, ApJ, 565, 208
Pei, Y. C. 1992, ApJ, 395, 130
Peng, C. Y., Impey, C. D., Rix, H.-W., Keeton, C. R., Falco, E. E., Kochanek, C. S., Lehar, J., & McLeod, B. A. 2006, in press [astro-ph/0601391]
Pérez-González, P. G., et al. 2005, ApJ, 630, 82
Perola, G. C., Matt, G., Cappi, M., Fiore, F., Guainazzi, M., Maraschi, L., Petrucci, P. O., & Piro, L. 2002, A&A, 389, 802
Richards, G. T., et al. 2005, MNRAS, 360, 839
Richards, G. T., et al. 2006a, ApJ, in press [astro-ph/0601434]
Richards, G. T., et al. 2006b, ApJS, in press [astro-ph/0601558]
Richstone, D. et al. 1998, Nature, 395, A14
Risaliti, G., & Elvis, M. 2005, ApJ, 629, L17
Roberts, M. S., & Haynes, M. P. 1994, ARA&A, 32, 115
Robertson, B., Yoshida, N., Springel, V., & Hernquist, L. 2004, ApJ, 606, 32
Robertson, B., Hernquist, L., Bullock, J.S., Cox, T.J., Di Matteo, T., Springel, V., & Yoshida, N. 2005, ApJ, submitted [astro-ph/0503369]
Robertson, B., Cox, T. J., Hernquist, L., Franx, M., Hopkins, P. F., Martini, P., & Springel, V. 2006a, ApJ, 641, 21
Robertson, B., Hernquist, L., Cox, T. J., Di Matteo, T., Hopkins, P. F., Martini, P., & Springel, V. 2006b, ApJ, 641, 90
Rothberg, B., & Joseph, R. D. 2004, AJ, 128, 2098
Rothberg, B., & Joseph, R. D. 2006, AJ, 131, 185
Rownd, B. K., & Young, J. S. 1999, AJ, 118, 670
Salpeter, E. E. 1955, ApJ, 121, 161
Salpeter, E. E. 1964, ApJ, 140, 796
Sánchez, S. F., Becker, T., Garcia-Lorenzo, B., Benn, C. R., Christensen, L., Kelz, A., Jahnke, K., & Roth, M. M. 2005, A&A, 429, L21
Sánchez, S. F., et al. 2004, ApJ, 614, 586
Sánchez, S. F., & González-Serrano, J. I. 2003, A&A, 406, 435
Sanders, D.B. et al. 1986, ApJ, 305, L45
Sanders, D.B. et al. 1988a, ApJ, 325, 74
Sanders, D.B. et al. 1988b, ApJ, 324, L55
Sanders, D.B. et al. 1988c, ApJ, 328, L35
Sanders, D. B. & Mirabel, I. F. 1996, ARA&A, 34, 749
Sargent, A.I. et al. 1987, ApJ, 312, L35
Sargent, A.I., Sanders, D.B. & Phillips, T.G. 1989, ApJ, 346, L9
Schweizer, F. 1982, ApJ, 252, 455
Schweizer, F. 1998, in Galaxies: Interactions and Induced Star Formation, eds. D. Friedli, L. Martinet & D. Pfenniger (Springer-Verlag, Berlin)
Scoville, N.Z. et al. 1986, ApJ, 311, L47
Shier, L. M., & Fischer, J. 1998, ApJ, 497, 163
Small, T. A., & Blandford, R. D. 1992, MNRAS, 259, 725
Soares, D. S. L., de Souza, R. E., de Carvalho, R. R., & Couto da Silva, T. C. 1995, A&A, 110, 371
Soifer, B.T. et al. 1984a, ApJ, 278, L71
Soifer, B.T. et al. 1984b, ApJ, 283, L1
Soifer, B.T., Houck, J.R. & Neugebauer, G. 1987, ARA&A, 25, 187
Somerville, R. S., Primack, J. R., & Faber, S. M. 2001, MNRAS, 320, 504
Somerville, R. S., et al. 2004a, ApJ, 600, L135
Somerville, R. S., Lee, K., Ferguson, H. C., Gardner, J. P., Moustakas, L. A., & Giavalisco, M. 2004b, ApJ, 600, L171
Springel, V. 2005, MNRAS, 364, 1105
Springel, V., Di Matteo, T., & Hernquist, L. 2005a, ApJ, 620, L79
Springel, V., Di Matteo, T., & Hernquist, L. 2005b, MNRAS, 361, 776
Springel, V. & Hernquist, L. 2002, MNRAS, 333, 649
Springel, V. & Hernquist, L. 2003a, MNRAS, 339, 289
Springel, V. & Hernquist, L. 2003b, MNRAS, 339, 312
Springel, V. & Hernquist, L. 2005, ApJ, 622, L9
Stockton, A. 1978, ApJ, 223, 747
Stockton, A. & MacKenty, J. 1987, ApJ, 316, 584
Stockton, A. & Ridgway, S. 1991, AJ, 102, 488
Strateva, I. V., Brandt, W. N., Schneider, D. P., Vanden Berk, D. G., & Vignali, C. 2005, AJ, 130, 387
Straughn, A. N., Cohen, S. H., Ryan, R. E., Hathi, N. P., Windhorst, R. A., & Jansen, R. A. 2006, ApJ, 639, 724
Sulentic, J. W., & Rabaca, C. R. 1994, ApJ, 429, 531
Surace, J. A., Sanders, D. B., & Evans, A. S. 2000, ApJ, 529, 170
Tacconi, L. J., Genzel, R., Lutz, D., Rigopoulou, D., Baker, A. J., Iserlohe, C., & Tecza, M. 2002, ApJ, 580, 73
Telfer, R. C., Zheng, W., Kriss, G. A., & Davidsen, A. F. 2002, ApJ, 565, 773
Toledo, H. M. H., Dultzin-Hacyan, D., Gonzalez, J. J., & Sulentic, J. W. 1999, AJ, 118, 108
Toomre A., 1977, in Evolution of Galaxies and Stellar Populations, 401, Yale Univ. Obs: New Haven
Toomre A. & Toomre J., 1972, ApJ, 178, 623
Ueda, Y., Akiyama, M., Ohta, K., & Miyaji, T. 2003, ApJ, 598, 886
Urrutia, T., Lacy, M., Gregg, M. D., & Becker, R. H. 2005, ApJ, 627, 75
Vanden Berk, D. E., et al. 2001, AJ, 122, 549
Vanden Berk, D. E., et al. 2006, AJ, 131, 84
van Dokkum, P. G. 2005, AJ, 130, 2647
Viel, M., Matarrese, S., Theuns, T., Munshi, D. & Wang, Y. 2003, MNRAS, 340, L47
Viel, M., Haehnelt, M.G. & Springel, V. 2004, MNRAS, 354, 684
Vignali, C., Brandt, W. N., & Schneider, D. P. 2003, AJ, 125, 433
Vitvitska, M., Klypin, A. A., Kravtsov, A. V., Wechsler, R. H., Primack, J. R., & Bullock, J. S. 2002, ApJ, 581, 799
Volonteri, M., Haardt, F., & Madau, P. 2003, ApJ, 582, 559
Walker, I. R., Mihos, J. C., & Hernquist, L. 1996, ApJ, 460, 121
Wilkes, B. J., Tananbaum, H., Worrall, D. M., Avni, Y., Oey, M. S., & Flanagan, J. 1994, ApJS, 92, 53

Wolf, C., et al. 2005, ApJ, 630, 771
Worthey, G., Faber, S. M., & Gonzalez, J. J. 1992, ApJ, 398, 69
Wyithe, J. S. B. & Loeb, A. 2003, ApJ, 595, 614
Xu, C., & Sulentic, J. W. 1991, ApJ, 374, 407
Xu, C. K., Sun, Y. C., & He, X. T. 2004, ApJ, 603, L73
Yee, H. K. C., & Ellingson, E. 1995, ApJ, 445, 37
Yip, C. W., et al. 2004, AJ, 128, 2603
Zepf, S. E., & Koo, D. C. 1989, ApJ, 337, 34
Zhang, Y., Anninos, P., & Norman, M. L. 1995, ApJ, 453, L57

TABLE 1
BEST-FIT OBSERVED MERGER LUMINOSITIES

	[1] $\langle M_{\rm BAND}\rangle = M_{10} + \alpha \log\left(\frac{M_{*,\rm new}}{10^{10}\,M_\odot}\right)$			[2] $\langle M_{\rm BAND}\rangle = M_{11} + \alpha \log\left(\frac{M_{*,\rm tot}}{10^{11}\,M_\odot}\right)$			[3] $\langle M_{\rm BAND}\rangle = M_8 + \alpha \log\left(\frac{M_{\rm BH}}{10^{8}\,M_\odot}\right)$			
Band	M_{10}	α	χ^2/ν	M_{11}	α	χ^2/ν	M_8	α	χ^2/ν	σ
280/40	-20.7 ± 0.1	-2.0 ± 0.1	0.61	-22.0 ± 0.2	-2.0 ± 0.3	2.29	-22.3 ± 0.2	-1.5 ± 0.2	2.76	0.62 ± 0.06
U	-19.7 ± 0.2	-2.0 ± 0.3	0.76	-20.9 ± 0.2	-2.3 ± 0.3	1.47	-21.3 ± 0.2	-1.9 ± 0.2	1.59	0.67 ± 0.32
B	-20.2 ± 0.2	-2.0 ± 0.2	0.97	-21.2 ± 0.1	-2.3 ± 0.2	0.83	-21.7 ± 0.1	-1.7 ± 0.2	0.77	0.49 ± 0.25
V	-20.7 ± 0.1	-2.0 ± 0.2	1.66	-21.6 ± 0.1	-2.2 ± 0.2	0.74	-22.1 ± 0.1	-1.7 ± 0.2	1.13	0.34 ± 0.28
R	-21.0 ± 0.1	-1.9 ± 0.2	2.40	-21.8 ± 0.1	-2.2 ± 0.2	0.88	-22.3 ± 0.1	-1.7 ± 0.1	1.61	0.52 ± 0.28
I	-21.2 ± 0.1	-1.9 ± 0.1	3.40	-21.9 ± 0.1	-2.3 ± 0.1	0.97	-22.5 ± 0.1	-1.7 ± 0.1	2.24	0.45 ± 0.26
J	-22.2 ± 0.1	-2.0 ± 0.1	6.40	-22.9 ± 0.1	-2.2 ± 0.1	1.51	-23.5 ± 0.1	-1.7 ± 0.1	3.69	0.47 ± 0.18
H	-22.6 ± 0.1	-2.1 ± 0.1	6.15	-23.4 ± 0.1	-2.2 ± 0.1	1.67	-24.1 ± 0.1	-1.7 ± 0.1	3.96	0.39 ± 0.17
K	-22.7 ± 0.1	-2.1 ± 0.1	5.18	-23.6 ± 0.1	-2.3 ± 0.1	1.47	-24.3 ± 0.1	-1.7 ± 0.1	3.42	0.29 ± 0.21
SDSS *u*	-19.3 ± 0.2	-2.2 ± 0.3	0.85	-20.7 ± 0.2	-2.2 ± 0.3	1.29	-21.1 ± 0.1	-1.7 ± 0.2	0.84	0.76 ± 0.41
SDSS *g*	-20.5 ± 0.2	-2.0 ± 0.2	1.15	-21.5 ± 0.1	-2.2 ± 0.2	0.80	-22.0 ± 0.1	-1.7 ± 0.2	0.85	0.52 ± 0.25
SDSS *r*	-20.9 ± 0.1	-1.9 ± 0.2	2.38	-21.7 ± 0.1	-2.2 ± 0.2	0.83	-22.3 ± 0.1	-1.7 ± 0.1	1.58	0.52 ± 0.27
SDSS *i*	-21.1 ± 0.1	-2.0 ± 0.1	3.19	-21.9 ± 0.1	-2.2 ± 0.1	0.88	-22.5 ± 0.1	-1.7 ± 0.1	2.08	0.48 ± 0.26
SDSS *z*	-21.3 ± 0.1	-2.0 ± 0.1	4.46	-22.0 ± 0.1	-2.3 ± 0.1	1.04	-22.6 ± 0.1	-1.7 ± 0.1	2.65	0.48 ± 0.22

[1]Distribution of observed luminosities of mergers, as a function of new stellar mass $M_{*,\rm new}$ formed during the merger. This assumes the probability of viewing a merger at some magnitude in the given band is a Gaussian with median $\langle M_{\rm BAND}\rangle$ and dispersion σ in the band.
[2]Same, as a function of total, final stellar mass $M_{*,\rm tot}$ after the merger.
[3]Same, as a function of final black hole mass $M_{\rm BH}$ after the merger.